This article has been accepted for publication in IEEE Internet of Things Journal. This is the author's version which has not been fully edited and content may change prior to final publication. Citation information: DOI 10.1109/JIOT.2025.3602496



# Optimizing RIS Placement for Joint Communication and Illumination in NOMA-Based VLC Systems

Xingwang Wang, Junhong Huang, Yafeng Sun, Jiatong Tu, and Kun Yang, *Fellow, IEEE*

***Abstract*—Reconfigurable Intelligent Surfaces (RISs) and Non-Orthogonal Multiple Access (NOMA) can enhance Visible Light Communication (VLC) systems by mitigating signal blockage and improving spectrum utilization. While boosting communication efficiency is crucial, maintaining high illumination quality is equally important. This paper investigates a novel approach to simultaneously improving the sum rate (SR) and illumination uniformity (IU) in a RIS-assisted NOMA-based VLC system. Communication and illumination optimization problems are formulated as a non-convex mixed-integer non-linear programming problem, considering RIS placement, LED-user association, and power allocation. To the best of our knowledge, this is the first work to jointly optimize SR and IU with explicit consideration of RIS placement. We propose a joint optimization approach that leverages a differential evolution algorithm to optimize RIS placement. During each iteration, the obtained solutions are further refined using a block coordinate descent algorithm, which iteratively solves the decomposed sub-problems of LED-user association and power allocation. Simulation results show that the approach outperforms existing methods in both SR and IU. Moreover, RIS placement optimization is shown to be crucial, as neglecting it significantly degrades performance. Finally, the impacts of noise power and total LED power are analyzed, offering practical insights for parameter selection in VLC systems.**

***Index Terms*—Reconfigurable Intelligent Surfaces (RIS), non-orthogonal multiple access (NOMA), visible light communication (VLC), illumination uniformity, joint optimization.**

## I. Introduction

VISIBLE Light Communication (VLC) has garnered significant attention in the development of wireless communication systems due to its high transmission rate, spectral efficiency, and energy efficiency. It utilizes high-speed switching light-emitting diodes (LEDs) as the transmitter to modulate the data into the generated light. At the receiver, the photodiodes (PDs) converts the detected light intensity into a voltage and demodulate information. Therefore, VLC can provide transmitting data while simultaneously offering illumination [1]. Utilizing these unique characteristics, VLC has been widely applied in indoor scenarios [2], underwater communications [3], vehicular communications [4], and is expected to be a key technology for future communication systems.

However, VLC still faces two critical challenges. The first is the signal blockage problem [5] caused by obstacles in non-line-of-sight (NLoS) scenarios, which can significantly degrade system's quality of service (QoS) [6], [7]. The second challenge is the increasing demand for high-capacity networks driven by the Internet of Things (IoT), which puts enormous pressure on VLC systems, as limited bandwidth and interference from multiple light sources can hinder communication. A promising solution to mitigate signal blockage is the use of reconfigurable intelligent surfaces (RISs) [8], [9]. RISs leverage passive elements such as mirrors or metasurfaces to dynamically control signal propagation, enabling the establishment of alternative line-of-sight (LoS) paths [10]. Moreover, Non-Orthogonal Multiple Access (NOMA) [8], [11] has emerged as a key technology to enhance spectrum efficiency by allowing multiple users to share the same frequency resource. By combining RIS to improve channel quality and NOMA for efficient spectrum utilization, RIS-assisted NOMA-based VLC systems can significantly enhance performance, reliability, and capacity. This combination makes them particularly well-suited to meet the growing demands of modern wireless communication.

Although there have been several works on RIS-assisted NOMA-based VLC systems to enhance communication performance, few studies have addressed the equally crucial aspect of illumination quality. The uneven illumination in common indoor environments such as workplaces and homes not only affects visual comfort but also poses a threat to human health. Therefore, it is critical to jointly optimize both sum rate (SR) and illumination uniformity (IU). While existing works primarily focus on improving performance metrics such as secrecy rate (SeR) [12], [13], bit-error rate (BER) [14], SR [15]–[20], and energy efficiency (EE) [15], [16]. In [12] and [13], the problem of maximizing the SeR for a trusted user while ensuring minimum rate constraints for untrusted users was formulated and solved by jointly optimizing power allocation and RIS configuration. Similarly, [19] utilized this approach to enhance the SR. To reduce the system's BER, [14] proposed a framework for jointly optimizing NOMA and RIS parameters, including decoding order, transmit power, and reflection coefficients. Both [15] and [16] explored optimization strategies to simultaneously improve the SR and EE by

This work was supported in part by the National Natural Science Foundation of China (NSFC) under Grant 62132004; and in part by the National Key Research and Development Program of China under Grant 2023YFB4502304. *(Corresponding author: Junhong Huang.)*

Xingwang Wang is with the College of Computer Science and Technology, Key Laboratory of Symbolic Computation and Knowledge Engineering of Ministry of Education, Jilin University, Changchun 130012, China (e-mail: xww@jlu.edu.cn).

Junhong Huang, Yafeng Sun, and Jiatong Tu are with the College of Computer Science and Technology, Jilin University, Changchun 130012, China (e-mail: huangjh23@mails.jlu.edu.cn; yfsun22@mails.jlu.edu.cn; tujt22@mails.jlu.edu.cn).

Kun Yang is with the School of Intelligent Software and Engineering, Nanjing University, Suzhou 210093, Jiangsu, China, and also with the School of Computer Science and Electronic Engineering, University of Essex, CO43SQ Colchester, U.K. (e-mail: kyang@ieee.org).

Authorized licensed use limited to: JILIN UNIVERSITY. Downloaded on August 29,2025 at 04:28:18 UTC from IEEE Xplore. Restrictions apply.
© 2025 IEEE. All rights reserved, including rights for text and data mining and training of artificial intelligence and similar technologies. Personal use is permitted, but republication/redistribution requires IEEE permission. See https://www.ieee.org/publications/rights/index.html for more information.

This article has been accepted for publication in IEEE Internet of Things Journal. This is the author's version which has not been fully edited and content may change prior to final publication. Citation information: DOI 10.1109/JIOT.2025.3602496



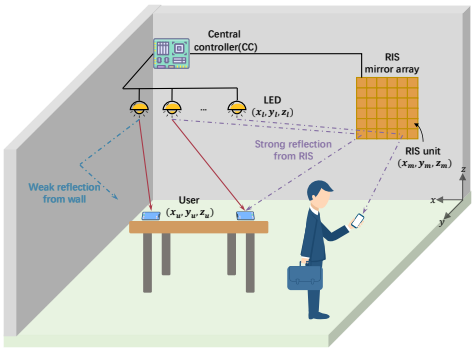


Fig. 1. System model of the RIS-assisted NOMA-based VLC

adjusting the roll and yaw angles of the reflector elements. The work in [20] further extended this by focusing specifically on improving the SR in mirror-based RIS-assisted VLC systems. In [17], the problem of maximizing the SR was addressed through joint optimization of active beamforming at LEDs and passive beamforming at the RIS, with a focus solely on RIS configuration. Building on this, [18] extended the approach by incorporating the decoding order in successive interference cancellation (SIC) as an additional factor in the optimization.

Moreover, RIS placement, which includes determining the physical location of the RIS array and the deployment of individual RIS units, is also a critical factor in the communication and illumination optimization of VLC systems. The RIS array position defines the origin of the RIS grid on the wall, while the unit deployment determines the reflection pattern. These factors directly influence the signal quality and illumination coverage. Unfortunately, the aforementioned works [12]–[20] overlook the optimization of RIS placement, focusing primarily on RIS configuration (e.g., phase shifts) or other factors. A notable exception is [21], which optimizes mirror placement on an entire wall to improve signal-to-interference-plus-noise ratio (SINR) while maintaining reasonable IU. However, [21] only considers optimizing the deployment of RIS units on the entire wall. It is not directly applicable due to size limitations and does not incorporate NOMA for enhanced system performance. Therefore, there is still a gap in the literature regarding the optimization of RIS placement for joint communication and illumination in size-constrained RIS-assisted NOMA-based VLC systems.

Motivated by the limitations discussed above, this paper investigates a RIS-assisted NOMA-based VLC system to simultaneously enhance communication efficiency and maintain high illumination quality, as depicted in Fig. 1. Moreover, RIS placement, LED-user association, and power allocation are tightly coupled factors influencing both SR and IU. Independently optimizing these variables may lead to sub-optimal trade-offs or infeasible configurations. Hence, we propose a joint optimization framework to simultaneously improve SR and IU. Table I compares our proposed work to related works. Specifically, the main contributions are as follows:

- To the best of our knowledge, this work is the first to simultaneously maximize both SR and IU in RIS-assisted NOMA-based VLC systems, while explicitly considering the RIS placement, including array position and unit deployment. This has significant implications for the practical implementation of VLC systems, as it addresses both communication performance and illumination quality, which are crucial for real-world applications. The optimization problem is formulated as a non-convex mixed-integer nonlinear programming (MINLP) problem, subject to several constraints, including LED-user association, total transmit power, individual QoS requirements, and the SIC decoding order.
- We propose a Joint optimization approach (JPAPA) to solve the problem, which optimizes RIS Placement, LED-user Association, and Power Allocation. Due to the coupling of decision variables involving different types, we first decompose the problem into two sub-problems of LED-user association and power allocation, assuming a fixed RIS placement. The differential evolution (DE) algorithm is employed to optimize the RIS placement, aiming to find the ideal array position and unit deployment. The obtained solutions are further refined using the block coordinate descent (BCD) algorithm, which iteratively solves the decomposed sub-problems. Specifically, the LED-user association is optimized using the projected gradient descent (PGD) algorithm based on semi-definite relaxation (SDR), while power allocation is optimized using the Broyden–Fletcher–Goldfarb–Shanno (BFGS) algorithm with Taylor expansion.
- Simulation results show that the proposed JPAPA outperforms several existing methods in terms of SR, and IU. Moreover, the results highlight the crucial role of RIS placement optimization, as neglecting it leads to significant performance degradation in both IU and SR. In typical scenarios with two or more users in the room, adding units to the RIS deployment improves both SR and IU, although some performance bottlenecks remain. Additionally, the simulation investigates the impact of noise power and total LED power, providing valuable insights for selecting ideal communication parameters in practical VLC systems.

The remainder of this article is organized as follows. The channel models of the LoS and RIS-reflected paths are discussed in Section II, and then the formulation of the problem is given in Section III. In Section IV, the algorithm is also presented. Then, detailed simulation results are shown in Section V. Finally, this article is concluded in Section VI.

*Notations:* $\mathbf{a}$ represents the vectors, and diag($\mathbf{a}$) is a diagonal matrix with the elements of the vector on the main diagonal. $\mathbb{R}_+$ denotes the positive real number set, and $(\cdot)^\top$ represents the transpose. Then, rank($\cdot$), vec($\cdot$), Tr($\cdot$) are the symbols of rank, vectorization operator, and trace, respectively. Moreover, $\|\cdot\|_1$, $\|\cdot\|_2$, $|\cdot|$ represent the 1-norm, 2-norm, and absolute value, respectively. $\odot$ and $\otimes$ denote Hadamard product and Kronecker product. If $F$ is a function with respect to $\mathbf{a}$, $\nabla_{\mathbf{a}} F$ represents the partial derivative of $F$ with respect to $\mathbf{a}$.

## II. System Models

Compared to conventional RF-based NOMA systems, implementing NOMA and SIC in VLC offers both unique chal-

Authorized licensed use limited to: JILIN UNIVERSITY. Downloaded on August 29,2025 at 04:28:18 UTC from IEEE Xplore. Restrictions apply.
© 2025 IEEE. All rights reserved, including rights for text and data mining and training of artificial intelligence and similar technologies. Personal use is permitted, but republication/redistribution requires IEEE permission. See https://www.ieee.org/publications/rights/index.html for more information.

This article has been accepted for publication in IEEE Internet of Things Journal. This is the author's version which has not been fully edited and content may change prior to final publication. Citation information: DOI 10.1109/JIOT.2025.3602496



TABLE I
LIST OF WORKS THAT CONSIDER PERFORMANCE OPTIMIZATION IN RIS-ASSISTED NOMA-BASED VLC SYSTEMS

| [#] | RIS Type | | | Objective Functions | | | | | Optimization aspect | | | | | |
|---|---|---|---|---|---|---|---|---|---|---|---|---|---|---|
| | Mirror array | Meta-surface | STAR-RIS | SeR | BER | SR | EE | IU | Units to AP/User Assignment | RIS Placement | Units Orientation | Units Configuration | Power Allocation | Decoding Order |
| [12] | ✓ | | | ✓ | | | | | ✓ | | | | ✓ | |
| [13] | ✓ | | | ✓ | | | | | ✓ | | | | ✓ | |
| [14] | | ✓ | | | ✓ | | | | | | | ✓ | ✓ | ✓ |
| [15] | | | ✓ | | | ✓ | ✓ | | | | ✓ | ✓ | | |
| [16] | | | ✓ | | | ✓ | ✓ | | ✓ | | | ✓ | | |
| [17] | | ✓ | | | | ✓ | | | ✓ | | | | | |
| [18] | ✓ | | | | | ✓ | | | ✓ | | | | | ✓ |
| [19] | | ✓ | | | | ✓ | | | ✓ | | | | ✓ | |
| [20] | ✓ | | | | | ✓ | | | | | ✓ | ✓ | | |
| This work | ✓ | | | | | ✓ | | ✓ | | ✓ | | | ✓ | |

* STAR-RIS: Simultaneous transmission and reflection reconfigurable intelligent surface.

lenges and advantages. The quasi-static and deterministic nature of VLC channels dominated by LoS components enables more precise channel ordering and power allocation, which are critical for effective SIC decoding. In addition, the absence of Doppler effects and the limited user mobility typical of indoor VLC environments help lower SIC complexity and reduce the risk of error propagation. On the other hand, VLC imposes strict non-negativity and peak-power constraints on transmitted signals, which complicates power-domain NOMA implementation compared to RF systems. Additionally, optical channel gains vary sharply with user positions, making dynamic power allocation more sensitive.

In this work, as shown in Fig. 1, we consider an indoor RIS-assisted downlink VLC system, where a mirror-based RIS is deployed to assist $L$ LED transmitters in serving $U$ users equipped with PDs. This design aims to ensure that the SIC decoding order remains effective even under the inherent constraints of VLC. The transmit power of each LED is $p_l$ Watt, $l = \{1, \cdots, L\}$. The use of multiple LEDs serves three purposes: 1) improve the sum throughput rate for all users, 2) perform SIC by using LEDs paired with users, and 3) achieve uniform illumination within the room.

To enhance performance of the VLC system, a mirror-based RIS array is placed on the wall to reflect NLoS signals from LEDs. The RIS placement refers to both the 3D spatial location of the array within the room (i.e., its offset along the $x$, $y$, and $z$ axes) and the deployment configuration of mirror units within the RIS (i.e., which units contain reflective elements). Together, these determine the signal reflection paths and their effectiveness for communication and illumination. The RIS array consists of $M = N \times N$ units, arranged in a closely spaced grid, and each unit can hold one mirror at most. The user's PD gain is depended on the light intensity from three main directions: i) direct LoS beams from LEDs, ii) strong reflections from the RIS, and iii) weak reflections from the walls, as shown in Fig. 1. The ideal RIS placement, including its position and unit deployment, determines the light reflection paths and incident angles from LEDs to RIS units and from RIS units to users.

To measure the IU, $K$ fixed monitoring points are distributed inside the room according to the user preference. The IU at a given region of interest is determined by the light intensities measured at these points, which receive illumination from three principal directions.

**Remark 1.** *Since SIC requires prior knowledge of the user's channel state information (CSI), during the user's movement, we can divide it into T time slots, and the coordinates of the user are known under each time slot. We assume that the central controller (CC) acquires the necessary CSI via standard wireless signaling . Specifically, during each coherence interval, the devices periodically transmit uplink pilot signals [22]. The CC performs channel estimation based on these pilot observations. Similarly, due to practical constraints, the positions of the LEDs are fixed and pre-known.*

**Remark 2.** *Since weak reflections from the wall are negligible compared to strong reflections from the RIS units [7], we assume NLoS signal strength is only determined by the RIS reflections. Based on the locations and CSI of all users, the CC, mounted on the ceiling, can jointly control the RIS and LED.*

### A. LoS Channel Gains

Since the VLC channel gain can be characterized by the Lambertian model, the LoS channel gain between the $l$th LED and the $u$th user is given by [23]

$$g_{l,u}^{\mathrm{LoS}} = \begin{cases} \frac{(q+1)A_u}{2\pi d_{l,u}^2} \cos^q(\phi_{l,u}) \cos(\theta_{l,u}) g_f g_c, & 0 \le \theta_{l,u} \le \Theta, \\ 0, & \text{otherwise}, \end{cases} \tag{1}$$

where $q = -1/\log_2(\cos(\Phi_{1/2}))$, with $\Phi_{1/2}$ as the half-intensity radiation angle. $A_u$ is the physical area of the user node's PD, and $\Theta$ represents the semi-angle of the Field of View (FoV). $d_{l,u}$ is the distance between LED $l$ and user node $u$, $\phi_{l,u}$ and $\theta_{l,u}$ are the irradiance and incidence angles, respectively, as shown in Fig. 2. Besides, $g_f$ and $g_c = \eta^2/\sin^2(\Theta)$ are the gains of the optical filter and the non-imaging concentrator, respectively, where $\eta$ is the refractive index. For the sake of expression, a vector $\mathbf{g}_u^{\mathrm{LoS}} = [g_{1,u}^{\mathrm{LoS}}, \cdots, g_{L,u}^{\mathrm{LoS}}]^\top \in \mathbb{R}_+^{L\times 1}$ is adopted to represent the complete set of potential LoS channel gains for the $u$th user. The $\cos(\theta_{l,u}) = \frac{z_l - z_u}{d_{l,u}}$ [24], where

Authorized licensed use limited to: JILIN UNIVERSITY. Downloaded on August 29,2025 at 04:28:18 UTC from IEEE Xplore. Restrictions apply.
© 2025 IEEE. All rights reserved, including rights for text and data mining and training of artificial intelligence and similar technologies. Personal use is permitted, but republication/redistribution requires IEEE permission. See https://www.ieee.org/publications/rights/index.html for more information.

This article has been accepted for publication in IEEE Internet of Things Journal. This is the author's version which has not been fully edited and content may change prior to final publication. Citation information: DOI 10.1109/JIOT.2025.3602496



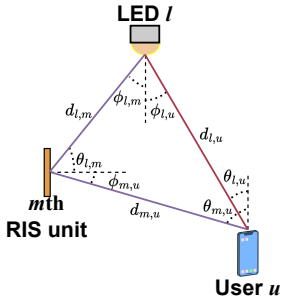


Fig. 2. The LoS and NLoS path of the RIS-assisted VLC system.

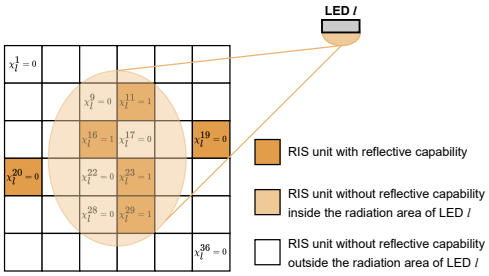


Fig. 3. The deployment of the mirrors on the RIS units, and the radiation area of the LED $l$.

$(x_l, y_l, z_l)$ and $(x_u, y_u, z_u)$ denote the position of the $l$th LED and the $u$th user at t slot, respectively.

### B. Non-LoS Channel Gains

As already assumed, we only consider strong reflections of the LoS light beams to obtain the NLoS gains. The potential NLoS channel gain between the $l$th LED and the $u$th user through the $m$th RIS unit can be expressed as [25]:

$$h_{l,m,u} = \begin{cases} \frac{\rho(q+1)A_u A_m d_{l,u}}{2\pi^2 d_{l,m}^2 d_{m,u}^2} \cos^q(\phi_{l,m}) \cos(\theta_{l,m}) \\ \quad \times \cos(\phi_{m,u}) \cos(\theta_{m,u}) g_f g_c, & 0 \le \theta_{m,u} \le \Theta, \\ 0, & \text{otherwise}, \end{cases} \tag{2}$$

where $\rho$ and $A_m$ represent the reflection factor [26] and physical area of the RIS unit, respectively. $d_{l,m}$ and $d_{m,u}$ denote the distances between the $l$th LED and the $m$th RIS unit, and between the $m$th RIS unit and the $u$th user, as shown in Fig. 2. $\phi_{l,m}$ and $\theta_{l,m}$ are the irradiance and incidence angles from the $l$th LED to the $m$th RIS unit, respectively. Similarly, $\phi_{m,u}$ and $\theta_{m,u}$ represent the irradiance angle from the $m$th RIS unit to the $u$th user and the incidence angle of the reflected signal, respectively. The cosine of the irradiance angle is expressed as $\cos(\theta_{m,u}) = \frac{y_m - y_u}{d_{m,u}}$ [27], where $(x_m, y_m, z_m)$ denotes the position of the $m$th unit. A vector $\mathbf{h}_{l,u} = [h_{l,1,u}, \cdots, h_{l,M,u}] \in \mathbb{R}_+^{1\times M}$ represents the complete set of potential NLoS channel gains for the $l$th LED toward to $u$th user. In addition, the LoS and NLoS gains of the monitoring points also can be computed by the Eq. (1) and Eq. (2), respectively.

The position of the RIS array determines where the RIS should be placed, and further determines the NLOS channel gains for the user according to Eq. (2). It is worth noting that the positions of all RIS units do not need to be represented individually. Instead, the position matrix $\mathbf{\Xi}$ can be derived from an initial position matrix $\mathbf{S}$ and an offset vector $\mathbf{w} = [\Delta x, \Delta y, \Delta z]$ as follows:

$$\mathbf{\Xi} = \mathbf{S} + \mathbf{w}. \tag{3}$$

where $\mathbf{S} \in \mathbb{R}_+^{M\times 3}$ is a fixed matrix where the position of the first RIS unit is at the origin. It represents the grid layout of the RIS units, which is defined as follows:

$$\mathbf{S} = \begin{bmatrix} 0 & 0 & 0 \\ & \cdots & \\ a\times(N-1) & 0 & 0 \\ 0 & 0 & -a\times 1 \\ & \cdots & \\ a\times(N-1) & 0 & -a\times 1 \\ & \cdots & \\ 0 & 0 & -a\times(N-1) \\ & \cdots & \\ a\times(N-1) & 0 & -a\times(N-1) \end{bmatrix}. \tag{4}$$

In this layout, the RIS units are numbered from top to bottom, left to right, with a side length of $a$. The second column of $\mathbf{S}$ is set to zero, indicating that the RIS array is placed on the wall as shown in Fig. 1. This layout can be adjusted based on user preferences by modifying the offset vector $\mathbf{w}$, which allows for the translation of the entire RIS array along the $x$, $y$, and $z$-axes.

### C. Total Channel Gains

As considered in [21], our work also introduces the notion of radiation area, since it is considered that the light from the LEDs does not necessarily cover all the RIS units completely. As shown in Fig. 3, the unit deployment determines which units possess the reflection capability, and further determines the actual NLOS channel gains. Thus, potential NLoS channel gain $g_{l,u}^{\text{NLoS}}$ of the $l$th LED toward to $u$th user, which can be computed by:

$$g_{l,u}^{\text{NLoS}} = \mathbf{h}_{l,u} \boldsymbol{\chi}_l^\top, \tag{5}$$

where $\boldsymbol{\chi}_l = [\chi_{l,1}, \cdots, \chi_{l,M}] \in \{0,1\}^{1\times M}$, such that

$$\chi_{l,m} = \begin{cases} \zeta_m, & \text{if } m \in \Upsilon_l, \\ 0, & \text{otherwise}, \end{cases} \tag{6}$$

where $\Upsilon_l$ represents the set of RIS unit indices within the radiation area of $l$th LED, determined by the angle between units and LEDs. Specifically, the $m$th RIS unit is considered to be within the radiation area of the $l$th LED if the irradiance angle $\phi_{l,m}$ from $l$th LED to $m$th RIS unit is less than or equal to the LED's half-intensity radiation angle $\Phi_{1/2}$. Therefore, if the $m$th unit is outside the radiation area of the $l$th LED ($m \notin \Upsilon_l$), then $\chi_{l,m} = 0$, meaning the unit does not reflect light. The binary variable $\chi_{l,m}$ depends on $\zeta_m$, where $\zeta_m = 1$ if a mirror is placed at the $m$th unit and $\zeta_m = 0$ otherwise. So,

Authorized licensed use limited to: JILIN UNIVERSITY. Downloaded on August 29,2025 at 04:28:18 UTC from IEEE Xplore. Restrictions apply.
© 2025 IEEE. All rights reserved, including rights for text and data mining and training of artificial intelligence and similar technologies. Personal use is permitted, but republication/redistribution requires IEEE permission. See https://www.ieee.org/publications/rights/index.html for more information.

This article has been accepted for publication in IEEE Internet of Things Journal. This is the author's version which has not been fully edited and content may change prior to final publication. Citation information: DOI 10.1109/JIOT.2025.3602496



if $\chi_{l,m} = 1$, the NLoS signal from the $l$th LED is considered. A vector $\mathbf{g}_u^{\text{NLoS}} = [g_{1,u}^{\text{NLoS}}, \cdots, g_{L,u}^{\text{NLoS}}]^\top \in \mathbb{R}_+^{L\times 1}$ represents the complete set of potential NLoS channel gains for the $u$th user.

Further, the total actual gain at the $u$th user is given by:

$$G_u = \mathbf{g}_u^\top \boldsymbol{\lambda}_u, \tag{7}$$

where $\mathbf{g}_u = \mathbf{g}_u^{\text{LoS}} + \mathbf{g}_u^{\text{NLoS}}$ represents the combined LoS and NLoS gains, and $\boldsymbol{\lambda}_u = [\lambda_{1,u}, \cdots, \lambda_{L,u}]^\top$ denotes the association between the $u$th user and LEDs. Here, $\lambda_{l,u} = 1$ indicates that the $u$th user is associated with the $l$th LED, and $\lambda_{l,u} = 0$ otherwise.

### D. Received Signals

In a multi-LED indoor VLC system with $U$ users, where CSI is obtained via channel estimation techniques [22], the received signal at the $u$th user under the NOMA principle is:

$$\begin{aligned} y_u = \mathbf{g}_u^\top(\boldsymbol{\lambda}_u \odot \boldsymbol{p})s_u + \sum_{j=1}^{U-1} \mathbf{g}_u^\top(\boldsymbol{\lambda}_j \odot \boldsymbol{p})s_j \\ + \sum_{i=u+1}^{U} \mathbf{g}_u^\top(\boldsymbol{\lambda}_i \odot \boldsymbol{p})s_i + n_0, \end{aligned} \tag{8}$$

where $\boldsymbol{p} = [p_1, \cdots, p_L]^\top$ denotes the LED power vector, and $n_0 \sim \mathcal{N}(0, \delta^2)$ is the additive white Gaussian noise. The first, second, and third terms represent the desired signal, interference canceled by SIC, and residual interference after SIC, respectively.

## III. Problem Formulation and Analysis

This work considers a fixed number of LEDs in an indoor VLC system, performing simultaneous communication and illumination with the assistance of an RIS array, as shown in Fig. 1. As shown in Table I, the SR is a key performance indicator for the VLC system. The achievable data rate $R_u$ of the $u$th user is given by [28]:

$$R_u = \frac{B}{2}\log_2\left(1 + \Gamma_u\right), \tag{9}$$

where $B$ is the modulation bandwidth, and $\Gamma_u$ is the SINR at the $u$th user. According to the definition of SINR provided in [29], we modify it to suit the problem discussed in this paper. expressed as

$$\Gamma_u = \frac{\left|\mathbf{g}_u^\top(\boldsymbol{\lambda}_u \odot \boldsymbol{p})\right|^2}{\frac{2\pi\delta^2}{e} + \sum\limits_{G_n > G_u} \left|\mathbf{g}_u^\top(\boldsymbol{\lambda}_n \odot \boldsymbol{p})\right|^2}, \tag{10}$$

where $e$ is the base of natural logarithms. The numerator represents the total intensity of the desired signals derived from both LoS and NLoS, while the denominator includes interference from users with better channel gains than the $u$th user ($G_n > G_u$), as well as ambient noise ($\frac{2\pi\delta^2}{e}$).

**Remark 3.** *In calculating the above, we follow three assumptions: i) time synchronization and ignoring propagation delay, ii) linear addition of signal strength, and iii) constant ambient light.*

Thus, the SR of the system is defined as:

$$SR = \sum_{u=1}^{U} R_u. \tag{11}$$

In addition, IU is also crucial in indoor environments, as uneven illumination can affect both lighting performance and human eyesight. Following [30], IU is quantified using the mean and variance of the illumination intensity at $K$ monitoring points. The total channel gains from all LEDs to the monitoring points are represented by matrix $\mathbf{H} = [g_{l,k} + h_{l,k}]_{L\times K}$, and the optical power vector is $\mathbf{q} = \varrho\mathbf{H}^\top\boldsymbol{p}$, where $\varrho$ denotes the luminous efficiency, e.g. $\varrho = 60$ lumen/watt for white LED. Thus, for quantifying the IU, the coefficient of variation of the root mean square error (CV(RMSE)) is defined by the ratio of the standard deviation to the mean value as

$$\Omega = \frac{\sqrt{K\|\mathbf{q}\|_2^2 - \|\mathbf{q}\|_1^2}}{\|\mathbf{q}\|_1}. \tag{12}$$

Joint optimization of RIS placement (position $\mathbf{w}$ and unit deployment $\boldsymbol{\zeta}$), LED-user association ($\boldsymbol{\lambda}$), and LED power allocation ($\boldsymbol{p}$) is crucial for maximizing both SR and IU. These elements are highly interdependent and significantly impact performance. RIS placement directly determines NLoS channel gains, affecting SINR and SR while also shaping the spatial light distribution critical for IU. LED-user association governs NOMA resource allocation, defines the SIC decoding order, and influences interference patterns. Power allocation requires a delicate trade-off between enhancing SR and maintaining uniform illumination across monitoring points. Crucially, these optimizations are mutually dependent. Optimal RIS placement depends on the user association strategy and power allocation, effective user association is constrained by RIS-influenced channel conditions and available power, and efficient power allocation relies on RIS-determined channel gains and association-defined interference patterns. Consequently, optimizing any single variable in isolation leads to suboptimal performance, as improvements in one factor are inherently constrained by the others.

Therefore, the joint optimization is essential to exploit synergies and effectively balance the dual objectives under practical constraints. We formulate the following multi-objective optimization problem $\mathbf{P}$:

$$\mathbf{P}: \quad \max_{\mathbf{w},\boldsymbol{\zeta},\boldsymbol{\lambda},\boldsymbol{p}} \{SR, -\Omega\} \tag{13a}$$

$$\text{s.t.} \quad R_u \geq R_{\min}, \forall u, \tag{13b}$$

$$\sum_{l=1}^{L} p_l \leq p_{\text{total}}, \tag{13c}$$

$$\left|\mathbf{g}_u^\top(\boldsymbol{\lambda}_i \odot \boldsymbol{p})\right|^2 \geq \left|\mathbf{g}_u^\top(\boldsymbol{\lambda}_j \odot \boldsymbol{p})\right|^2, \forall u, \forall G_i \leq G_j, \tag{13d}$$

$$\zeta_m \in \{0,1\}, \forall m, \tag{13e}$$

$$\lambda_{l,u} \in \{0,1\}, \forall l, \forall u, \tag{13f}$$

$$\sum_{u}^{U} \lambda_{l,u} \leq 1, \forall l, \tag{13g}$$

$$\mathbf{q} \geq \mu\mathbf{1}_{K\times 1}. \tag{13h}$$

Authorized licensed use limited to: JILIN UNIVERSITY. Downloaded on August 29,2025 at 04:28:18 UTC from IEEE Xplore. Restrictions apply.
© 2025 IEEE. All rights reserved, including rights for text and data mining and training of artificial intelligence and similar technologies. Personal use is permitted, but republication/redistribution requires IEEE permission. See https://www.ieee.org/publications/rights/index.html for more information.

This article has been accepted for publication in IEEE Internet of Things Journal. This is the author's version which has not been fully edited and content may change prior to final publication. Citation information: DOI 10.1109/JIOT.2025.3602496



Constraint (13b) ensures each user achieves a minimum rate $R_{\min}$ to meet QoS requirements, and (13c) enforces a power constraint, i.e., the total LED power is limited to $p_{\text{total}}$. Then, constraint (13d) ensures correct SIC operation and fairness in achievable data rates, assuming the users' channel gains have been ranked in ascending order. The binary variable $\zeta_m$ indicates whether a mirror is placed at the $m$th unit. Constraints (13f) and (13g) allow multiple LEDs to associate with a user, but each LED can only associate with one user at a time. Finally, the IU constraint in (13h) limits the minimum illumination level at monitoring points.

**Theorem 1.** *Problem* $\mathbf{P}$ *is a non-convex and NP-hard MINLP.*

*Proof.* The proof is given in Appendix A. □

## IV. The Proposed Algorithm

The problem formulated in Section III is a MINLP that is both non-convex and NP-hard. Solving it directly is computationally intractable. To address this, we decompose the problem into manageable sub-problems. Before that, we convert the multi-objective problem into a single-objective one to simplify complexity, unify evaluation criteria, and facilitate trade-offs between objectives. Next, assuming fixed RIS array position and unit deployment, we decompose the problem into two sub-problems, i.e., LED-user association and power allocation. The BCD method is employed to solve these sub-problems iteratively. Specifically, the LED-user association sub-problem is solved using the PGD algorithm based on SDR, while power allocation is optimized using the BFGS algorithm based on Taylor expansion. Additionally, a DE-based optimization is applied to solve the RIS placement problem, obtaining the ideal RIS array position and unit deployment.

### A. Problem Reformulation

Based on [31], we convert the multi-objective optimization problem into a single-objective problem using the right-of-use coefficient method. The objective function in Eq. (13a) becomes

$$\psi(\mathbf{w}, \boldsymbol{\zeta}, \boldsymbol{\lambda}, \boldsymbol{p}) = w_1 SR - w_2 \Omega, \tag{14}$$

where $w_1$ and $w_2$ are non-negative weight factors for the SR and CV(RMSE), respectively, and can be adjusted based on user preferences [32]. The multi-objective optimization problem $\mathbf{P}$ is thus transformed into a single-objective problem $\mathbf{P_1}$:

$$\mathbf{P_1}: \quad \max_{\mathbf{w},\boldsymbol{\zeta},\boldsymbol{\lambda},\boldsymbol{p}} \psi(\mathbf{w}, \boldsymbol{\zeta}, \boldsymbol{\lambda}, \boldsymbol{p}) \tag{15a}$$

$$\text{s.t.} \quad (13b)\text{-}(13h). \tag{15b}$$

This transformation simplifies the problem, mitigates discrepancies between objectives, and allows flexible adjustment of their relative importance. However, the problem $\mathbf{P_1}$ remains challenging due to the non-convex objective and constraints. To address this, we decompose $\mathbf{P_1}$ into two sub-problems of LED-user association, and power allocation based on the BCD method, assuming fixed RIS array position and unit deployment.

### B. LED-user association

Given the RIS array position $\widehat{\mathbf{w}} = [\Delta\widehat{x}, \Delta\widehat{y}, \Delta\widehat{z}]$ and unit deployment $\widehat{\boldsymbol{\zeta}} = \{\widehat{\zeta}_m, \forall m\}$, the LoS and NLoS channel gains are fixed, and the decoding order is determined. With the power allocation $\widehat{\boldsymbol{p}} = \{\widehat{p}_l, \forall l\}$, the LED-user association problem is expressed as:

$$\mathbf{P_{1.1}}: \quad \max_{\boldsymbol{\lambda}} \psi(\widehat{\mathbf{w}}, \widehat{\boldsymbol{\zeta}}, \boldsymbol{\lambda}, \widehat{\boldsymbol{p}}) \tag{16a}$$

$$\text{s.t.} \quad (13b), (13d), (13f), (13g). \tag{16b}$$

To simplify the objective function, we introduce some auxiliary variables. Let $\tilde{\boldsymbol{\lambda}} = \text{vec}(\boldsymbol{\lambda}) = [\lambda_1^\top, \cdots, \lambda_U^\top]^\top \in \mathbb{R}_+^{LU\times 1}$ denote the association vector, and define $\text{O}(u)$ as the decoding order of the $u$th user. Define two binary vectors $\mathbf{c}_u = [c_{u,1}, \cdots, c_{u,U}]^\top$ and $\bar{\mathbf{c}}_u = [\bar{c}_{u,1}, \cdots, \bar{c}_{u,U}]^\top$, where

$$c_{u,i} = \begin{cases} 1, & \forall\, \text{O}(u) \le \text{O}(i), \\ 0, & \text{otherwise}, \end{cases} \tag{17}$$

$$\bar{c}_{u,i} = \begin{cases} 1, & \forall\, \text{O}(u) < \text{O}(i), \\ 0, & \text{otherwise}. \end{cases} \tag{18}$$

Moreover, let $\mathbf{e}_u \in \mathbb{R}_+^{U\times 1}$ be a vector with 1 in the $u$th position and zeros elsewhere. Define the following auxiliary variables:

$$\mathbf{G}_u = \text{diag}(\mathbf{c}_u) \otimes \widehat{\mathbf{g}}_u \widehat{\mathbf{g}}_u^\top, \quad \forall u, \tag{19}$$

$$\bar{\mathbf{G}}_u = \text{diag}(\bar{\mathbf{c}}_u) \otimes \widehat{\mathbf{g}}_u \widehat{\mathbf{g}}_u^\top, \quad \forall u, \tag{20}$$

$$\mathbf{Z}_{i,u} = \text{diag}(\mathbf{e}_i) \otimes \widehat{\mathbf{g}}_u \widehat{\mathbf{g}}_u^\top, \quad \forall i, u, \tag{21}$$

$$b = (2^{2R_{\min}/B} - 1)\frac{2\pi\delta^2}{e}. \tag{22}$$

The matrices $\mathbf{G}_u$, $\bar{\mathbf{G}}_u$, and $\mathbf{Z}_{i,u}$ are all $LU \times LU$. Since $\widehat{\mathbf{g}}_u$ and $\widehat{\boldsymbol{p}}$ are fixed, $\Omega$ is a constant, denoted as $c$. The objective $SR$ can be written as

$$SR' = \sum_{u=1}^{U} \frac{B}{2} \log_2 \left( \frac{\frac{2\pi\delta^2}{e} + \tilde{\boldsymbol{\lambda}}^\top \mathbf{G}_u \tilde{\boldsymbol{\lambda}}}{\frac{2\pi\delta^2}{e} + \tilde{\boldsymbol{\lambda}}^\top \bar{\mathbf{G}}_u \tilde{\boldsymbol{\lambda}}} \right), \tag{23}$$

then the problem $\mathbf{P_{1.1}}$ is transformed as:

$$\mathbf{P'_{1.1}}: \quad \max_{\tilde{\boldsymbol{\lambda}}} \psi'(\widehat{\mathbf{w}}, \widehat{\boldsymbol{\zeta}}, \boldsymbol{\lambda}, \widehat{\boldsymbol{p}}) = w_1 SR' - w_2 c \tag{24a}$$

$$\text{s.t.} \quad \tilde{\boldsymbol{\lambda}}^\top \left( \mathbf{G}_u - 2^{2R_{\min}/B} \bar{\mathbf{G}}_u \right) \tilde{\boldsymbol{\lambda}} \ge b, \forall u, \tag{24b}$$

$$\tilde{\boldsymbol{\lambda}}^\top \mathbf{Z}_{i,u} \tilde{\boldsymbol{\lambda}} \ge \tilde{\boldsymbol{\lambda}}^\top \mathbf{Z}_{j,u} \tilde{\boldsymbol{\lambda}}, \forall u, \forall \text{O}(i) \le \text{O}(j), \tag{24c}$$

$$\tilde{\lambda}_i \in \{0, 1\}, \forall 1 \le i \le LU, \tag{24d}$$

$$\mathbf{A}\tilde{\boldsymbol{\lambda}} \le \mathbf{1}_{L\times 1}, \tag{24e}$$

where $\mathbf{1}_{L\times 1}$ represents an all-one vector of dimension $L \times 1$, and $\mathbf{A} \in \mathbb{R}_+^{L\times LU}$ is a matrix where the elements from $(i-1)L - 1$ to $iL$ in the $i$th row are all ones, and the rest are zeros. It is clear that the problem is a quadratic programming problem with quadratic constraints, which can be solved by

Authorized licensed use limited to: JILIN UNIVERSITY. Downloaded on August 29,2025 at 04:28:18 UTC from IEEE Xplore. Restrictions apply.
© 2025 IEEE. All rights reserved, including rights for text and data mining and training of artificial intelligence and similar technologies. Personal use is permitted, but republication/redistribution requires IEEE permission. See https://www.ieee.org/publications/rights/index.html for more information.

This article has been accepted for publication in IEEE Internet of Things Journal. This is the author's version which has not been fully edited and content may change prior to final publication. Citation information: DOI 10.1109/JIOT.2025.3602496



SDR. Therefore, the problem can be further transformed with $\mathbf{D}=\tilde{\boldsymbol{\lambda}}\tilde{\boldsymbol{\lambda}}^{\top}$ as follows:

$$\mathbf{P'_{1.1.1}}: \quad \max_{\mathbf{D}} w_1 \sum_{u=1}^{U} \frac{B}{2}\log_2\left(\frac{\frac{2\pi\delta^2}{e}+\mathrm{Tr}(\mathbf{D}\mathbf{G}_u)}{\frac{2\pi\delta^2}{e}+\mathrm{Tr}(\mathbf{D}\bar{\mathbf{G}}_u)}\right)-w_2 c \tag{25a}$$

$$\text{s.t.} \quad (24d), \tag{25b}$$

$$\mathrm{Tr}\left(\mathbf{D}\left(\mathbf{G}_u-2^{2R_{\min}/B}\bar{\mathbf{G}}_u\right)\right)\geq b,\forall u, \tag{25c}$$

$$\mathrm{Tr}\left(\mathbf{D}\mathbf{Z}_{i,u}\right)\geq \mathrm{Tr}\left(\mathbf{D}\mathbf{Z}_{j,u}\right),\forall u,\forall \mathrm{O}(i)\leq \mathrm{O}(j), \tag{25d}$$

$$\mathbf{A}\mathbf{D}\mathbf{1}_{LU\times 1}\leq \mathbf{1}_{L\times 1}, \tag{25e}$$

$$\mathbf{D}\succeq \mathbf{0}, \tag{25f}$$

$$\mathrm{rank}(\mathbf{D})=1, \tag{25g}$$

**Theorem 2.** *The satisfaction of constraint (25e) implies that constraint (24e) is also satisfied.*

*Proof.* The proof is given in Appendix B. □

Due to the objective function and the constraint in (25g) are still non-convex, the slack variables $v_u$ and $\bar{v}_u$ are introduced as follows:

$$e^{v_u}=\frac{2\pi\delta^2}{e}+\mathrm{Tr}(\mathbf{D}\mathbf{G}_u),\forall u, \tag{26}$$

$$e^{\bar{v}_u}=\frac{2\pi\delta^2}{e}+\mathrm{Tr}(\mathbf{D}\bar{\mathbf{G}}_u),\forall u. \tag{27}$$

Based on the above, the problem can be further rewritten as

$$\mathbf{P'_{1.1.2}}: \quad \max_{\mathbf{D},v_u,\bar{v}_u} w_1 \sum_{u=1}^{U} \frac{B\log_2 e}{2}(v_u-\bar{v}_u)-w_2 c \tag{28a}$$

$$\text{s.t.} \quad (25a)\text{-}(25g), \tag{28b}$$

$$e^{v_u}\leq \frac{2\pi\delta^2}{e}+\mathrm{Tr}(\mathbf{D}\mathbf{G}_u),\forall u, \tag{28c}$$

$$e^{\bar{v}_u}\geq \frac{2\pi\delta^2}{e}+\mathrm{Tr}(\mathbf{D}\bar{\mathbf{G}}_u),\forall u. \tag{28d}$$

However, (28c) is still non-convex because it have convex function on the left and linear function on the right. To convert the constraint into convex, the first-order Taylor expansion is applied to determine the lower bound at given local points $\bar{v}_u^*$, which be expressed as

$$e^{\bar{v}_u}\geq e^{\bar{v}_u^*}(\bar{v}_u-\bar{v}_u^*+1),\forall u. \tag{29}$$

Then, the problem $\mathbf{P'_{1.1.2}}$ can be approximated at given local points $\bar{v}_u^*$ as

$$\mathbf{P'_{1.1.3}}: \quad \max_{\mathbf{D},v_u,\bar{v}_u} w_1 \sum_{u=1}^{U} \frac{B\log_2 e}{2}(v_u-\bar{v}_u)-w_2 c \tag{30a}$$

$$\text{s.t.} \quad (25a)-(25g),(28c), \tag{30b}$$

$$e^{\bar{v}_u^*}(\bar{v}_u-\bar{v}_u^*+1)\geq \frac{2\pi\delta^2}{e}+\mathrm{Tr}(\mathbf{D}\bar{\mathbf{G}}_u),\forall u. \tag{30c}$$

If constraint (25g) is temporarily ignored, the problem becomes a convex semi-definite program (SDP). The integer constraint (25b) can be relaxed to $\tilde{\lambda}_i\in(0,1),\forall 1\leq i\leq LU$, and then transformed into binary variables using the threshold rounding method [33]. An initial matrix $\boldsymbol{\lambda}^{(0)}$ that satisfies the constraints can be computed from the value of $\bar{v}_u^*$. After these adjustments, the problem can be solved using the PGD algorithm [34]. After solving $\mathbf{P'_{1.1.3}}$ with PGD, update $\bar{v}_u^*$ with the latest solution $\bar{v}_u$, and adjust constraint (30c) accordingly. The algorithm terminates when $\bar{v}_u^*$ converges. Finally, $\tilde{\boldsymbol{\lambda}}$ can be obtained by solving the following problem:

$$\tilde{\boldsymbol{\lambda}}=\arg\min_{\tilde{\boldsymbol{\lambda}}}\|\mathbf{D}-\tilde{\boldsymbol{\lambda}}\tilde{\boldsymbol{\lambda}}^{\top}\|, \tag{31}$$

where $\tilde{\boldsymbol{\lambda}}=\sqrt{\nu_{\max}}\mathbf{f}$ is the closed-form solution, with $\nu_{max}$ being the largest eigenvalue of $\mathbf{D}$ and $\mathbf{f}$ its corresponding eigenvector. The pseudo-code for solving the LED-user association problem is summarized in Algorithm 1.

**Algorithm 1** Iterative Optimization Algorithm for LED-user Association Problem

**Input:** LED-user association $\boldsymbol{\lambda}^{(0)}$, slack variable $\bar{v}_u^{(0)}$, and iteration index $i$.
**Output:** Optimal LED-user association $\boldsymbol{\lambda}^*$.
1: **Initialization:** Set iteration index $i=0$, accuracy tolerance $\epsilon_1=10^{-4}$, initialized feasible association matrix $\boldsymbol{\lambda}^{(0)}$, and $\bar{v}_u^{(0)}$ computed with $\boldsymbol{\lambda}^{(0)}$ based on (27);
2: **repeat**
3: $\bar{v}_u^*\leftarrow\bar{v}_u^{(i)},\forall u$;
4: $i\leftarrow i+1$;
5: Solve the problem $\mathbf{P'_{1.1.3}}$ by the PGD algorithm and obtain $v_u^{(i)}$, $\bar{v}_u^{(i)}$, and $\mathbf{D}^i$;
6: **until** $\sum_{u=1}^{U}\left|\bar{v}_u^*-\bar{v}_u^{(i)}\right|\leq\epsilon_1$;
7: Obtain the association vector $\tilde{\boldsymbol{\lambda}}$ by solving (31);
8: **return** $\boldsymbol{\lambda}^*$.

### C. Power Allocation

Given the optimized association matrix $\boldsymbol{\lambda}^r=\{\lambda_{l,u}^r,\forall l,u\}$ and the updated channel gains $\mathbf{g}_u^r,\forall u$, the power allocation problem can be expressed as:

$$\mathbf{P_{1.2}}: \quad \max_{\boldsymbol{p}} \psi(\widehat{\mathbf{w}},\widehat{\boldsymbol{\zeta}},\boldsymbol{\lambda}^r,\boldsymbol{p}) \tag{32a}$$

$$\text{s.t.} \quad (13b)\text{-}(13d),(13h). \tag{32b}$$

Similarly, for simplifying the expression, the auxiliary variables of $\mathbf{G}_u^r$, $\bar{\mathbf{G}}_u^r$, and $\mathbf{Z}_{i,u}^r$ are also introduced based on (19), (20) and (21), respectively, with the difference that $\widehat{\mathbf{g}}_u$ is replaced by $\widehat{\mathbf{g}}_u\odot\boldsymbol{\lambda}^r$. Thus, the objective $SR$ can be written in the following equivalent form as

$$SR'=\sum_{u=1}^{U}\frac{B}{2}\log_2\left(\frac{\frac{2\pi\delta^2}{e}+\tilde{\boldsymbol{p}}^{\top}\mathbf{G}_u^r\tilde{\boldsymbol{p}}}{\frac{2\pi\delta^2}{e}+\tilde{\boldsymbol{p}}^{\top}\bar{\mathbf{G}}_u^r\tilde{\boldsymbol{p}}}\right), \tag{33}$$

where $\tilde{\boldsymbol{p}}=\mathrm{vec}(\boldsymbol{p}\odot\mathbf{1}_{L\times U})\in\mathbb{R}_+^{LU\times 1}$. Then, the problem $\mathbf{P_{1.2}}$ is transformed as:

$$\mathbf{P'_{1.2}}: \quad \max_{\boldsymbol{p}} \psi'(\widehat{\mathbf{w}},\widehat{\boldsymbol{\zeta}},\boldsymbol{\lambda},\widehat{\boldsymbol{p}})=w_1 SR'-w_2\Omega \tag{34a}$$

$$\text{s.t.} \quad \tilde{\boldsymbol{p}}^{\top}\left(\mathbf{G}_u^r-2^{2R_{\min}/B}\bar{\mathbf{G}}_u^r\right)\tilde{\boldsymbol{p}}\geq b,\forall u, \tag{34b}$$

$$\|\boldsymbol{p}\|_1\leq p_{\text{total}}, \tag{34c}$$

$$\tilde{\boldsymbol{p}}^{\top}\left(\mathbf{Z}_{i,u}^r-\mathbf{Z}_{j,u}^r\right)\tilde{\boldsymbol{p}}\geq 0,\forall u,\forall \mathrm{O}(i)\leq \mathrm{O}(j), \tag{34d}$$

$$\mathbf{q}\geq\mu\mathbf{1}_{K\times 1}. \tag{34e}$$

Authorized licensed use limited to: JILIN UNIVERSITY. Downloaded on August 29,2025 at 04:28:18 UTC from IEEE Xplore. Restrictions apply.
© 2025 IEEE. All rights reserved, including rights for text and data mining and training of artificial intelligence and similar technologies. Personal use is permitted, but republication/redistribution requires IEEE permission. See https://www.ieee.org/publications/rights/index.html for more information.

This article has been accepted for publication in IEEE Internet of Things Journal. This is the author's version which has not been fully edited and content may change prior to final publication. Citation information: DOI 10.1109/JIOT.2025.3602496



The subproblem $\mathbf{P'_{1.2}}$ shares a structural resemblance with the subproblem $\mathbf{P'_{1.1.3}}$ in its quadratic formulation. However, unlike $\mathbf{P'_{1.1.3}}$ where non-convexity arises from a low-rank matrix variable (amenable to SDR), the non-convexity of $\mathbf{P'_{1.2}}$ additionally stems from the non-specific form of $\Omega$ in the objective function and other constraints. Directly applying SDR to this type is not straightforward and often does not yield tight relaxations or a clear path to the optimal solution. To address this, we apply the first-order Taylor expansion, relaxing them as

$$(\tilde{\boldsymbol{p}}^*)^\top \mathbf{T}_u \tilde{\boldsymbol{p}}^* + 2(\tilde{\boldsymbol{p}}^*)^\top \mathbf{T}_u(\tilde{\boldsymbol{p}} - \tilde{\boldsymbol{p}}^*) \geq b, \forall u, \tag{35}$$

$$(\tilde{\boldsymbol{p}}^*)^\top \mathbf{K}^u_{i,j} \tilde{\boldsymbol{p}}^* + 2(\tilde{\boldsymbol{p}}^*)^\top \mathbf{K}^u_{i,j}(\tilde{\boldsymbol{p}} - \tilde{\boldsymbol{p}}^*) \geq 0, \forall u, \forall \mathrm{O}(i) \leq \mathrm{O}(j), \tag{36}$$

where $\tilde{\boldsymbol{p}}^* = \mathrm{vec}(\boldsymbol{p}^* \odot \mathbf{1}_{L\times U})$ given point $\boldsymbol{p}^*$, $\mathbf{T}_u = \mathbf{G}^r_u - 2^{2R_{\min}/B}\bar{\mathbf{G}}^r_u$, and $\mathbf{K}^u_{i,j} = \mathbf{Z}^r_{i,u} - \mathbf{Z}^r_{j,u}$, respectively. After this relaxation, all constraints become convex and linear, and the objective function remains smooth and differentiable. For such a problem with continuous variables and convexified constraints, the Augmented Lagrangian Method (ALM) integrated with BFGS is a highly effective and computationally efficient choice. ALM transforms the constrained optimization into a sequence of unconstrained subproblems by incorporating constraints into the objective function as penalty terms and Lagrangian multipliers, as shown in (37)-(40). BFGS, a quasi-Newton method, is then well-suited for solving these unconstrained, differentiable subproblems, providing efficient convergence for continuous variable optimization. This approach is preferred over SDR here because SDR's primary advantage lies in relaxing non-convexities arising from integer variables or rank constraints, which are not present in $\mathrm{P}'_{1.2}$ after Taylor expansion and its variables are continuous. Then, all constraints are convex and linear, while the objective function is smooth and differentiable. Moreover, we consider that the problem should be transformed into an equivalent constraint-free problem that is convenient to solve. Thus, all constraints are transformed to penalty terms based the augmented Lagrangian method (ALM) as

$$L_1 = \sum_{u=1}^{U} \xi^\alpha_u \left(b - Q_1(\tilde{\boldsymbol{p}})\right) + \frac{1}{2}\left(b - Q_1(\tilde{\boldsymbol{p}})\right)^2, \tag{37}$$

$$L_2 = \xi^\beta \left(\|\boldsymbol{p}\|_1 - p_{\text{total}}\right) + \frac{1}{2}\left(\|\boldsymbol{p}\|_1 - p_{\text{total}}\right)^2, \tag{38}$$

$$L_3 = \sum_{u=1}^{U}\sum_{i,j} \xi^\omega_{u,ij} Q_2(\tilde{\boldsymbol{p}}) + \frac{1}{2} Q_2^2(\tilde{\boldsymbol{p}}), \tag{39}$$

$$L_4 = \sum_{k=1}^{K} \xi^\gamma_k (\mu - \mathbf{q}_k) + \frac{1}{2}(\mu - \mathbf{q}_k)^2, \tag{40}$$

where $Q_1(\tilde{\boldsymbol{p}}) = (\tilde{\boldsymbol{p}}^*)^\top \mathbf{T}_u \tilde{\boldsymbol{p}}^* + 2(\tilde{\boldsymbol{p}}^*)^\top \mathbf{T}_u(\tilde{\boldsymbol{p}} - \tilde{\boldsymbol{p}}^*)$, and $Q_2(\tilde{\boldsymbol{p}}) = 2(\tilde{\boldsymbol{p}}^*)^\top \mathbf{K}^u_{i,j}(\tilde{\boldsymbol{p}}^* - \tilde{\boldsymbol{p}}) - (\tilde{\boldsymbol{p}}^*)^\top \mathbf{K}^u_{i,j}\tilde{\boldsymbol{p}}^*$.

For the convenience of expression, let $\boldsymbol{\xi} = \{\boldsymbol{\xi}^\alpha, \boldsymbol{\xi}^\beta, \boldsymbol{\xi}^\omega, \boldsymbol{\xi}^\gamma\}$. Therefore, the Lagrangian function is formulated as

$$F_\psi(\boldsymbol{p}, \boldsymbol{\xi}) = -w_1 SR' + w_2 \Omega + \sum_{i=1}^{4} L_i, \tag{41}$$

**Algorithm 2** Iterative Optimization Algorithm for Power Allocation Problem

**Input:** Power allocation $\boldsymbol{p}^{(0)}$, and iteration indexes $i$, $j$.
**Output:** Optimal power allocation $\boldsymbol{p}^*$.

**Initialization:** Set iteration index $i = 0$, $j = 0$, accuracy tolerances $\epsilon_2 = 10^{-4}$, $\epsilon_3 = 10^{-4}$, initialized feasible power vector $\boldsymbol{p}^{(0)}$;
**repeat**
  $j = 0$, $\boldsymbol{p}^* = \boldsymbol{p}^{(i)}$;
  **repeat**
    Calculate $\nabla_{\boldsymbol{p}} F^{(i)}_\psi$;
    Calculate $\mathbf{E}_{i,j}$ based on (42);
    Obtain optimal step size $\delta^*$ based on (43);
    Update $\boldsymbol{p}^{(i,j+1)}$ based on (44);
    $j \leftarrow j + 1$
  **until** $\|\boldsymbol{p}^{(i,j+1)} - \boldsymbol{p}^{(i,j)}\|_1 \leq \epsilon_2$
  $\boldsymbol{p}^{(i+1,0)} \leftarrow \boldsymbol{p}^{(i,j)}$;
  Update $\boldsymbol{\xi}^{(i+1)}$ based on (45);
  $i \leftarrow i + 1$;
**until** $\|\boldsymbol{\xi}^{(i+1)} - \boldsymbol{\xi}^{(i)}\|_1 \leq \epsilon_3$;
**return** $\boldsymbol{p}^*$.

which is a constraint-free problem can be solved by BFGS algorithms [35]. To avoid convergence to a local optimum, it's essential to run multiple attempts with different initial values to ensure finding the global optimum. First, the approximate inverse of the Hessian matrix is represented by the iterative formula as

$$\begin{aligned}\mathbf{E}_{i,j} &= \mathrm{BFGS}(\mathbf{E}_{i,j-1}, \Delta_1, \Delta_2) \\ &= \left[\mathbf{I} - \frac{\Delta_1 \Delta_2^\top}{\Delta_2^\top \Delta_1}\right] \mathbf{E}_{i,j-1} \left[\mathbf{I} - \frac{\Delta_2 \Delta_1^\top}{\Delta_2^\top \Delta_1}\right] + \frac{\Delta_1 \Delta_1^\top}{\Delta_2^\top \Delta_1},\end{aligned} \tag{42}$$

where $\Delta_1 = \boldsymbol{p}^{(i,j)} - \boldsymbol{p}^{(i,j-1)}$, $\Delta_2 = \nabla_{\boldsymbol{p}} F^{(i,j)}_\psi - \nabla_{\boldsymbol{p}} F^{(i,j-1)}_\psi$. $\mathbf{E}_{i,0} = \mathbf{I}$ is the identity matrix for initialization, and $i, j$ are ALM and BFGS iteration steps, respectively. Besides, the optimal step size at each iteration is determined by a one-dimensional line search based on the Armijo-Goldstein criterion [36], which is expressed as

$$\delta^* = \arg\min_{\delta} F_\psi(\boldsymbol{p}^{(i,j)} - \delta \mathbf{E}_{i,j} \nabla_{\boldsymbol{p}} F^{(i,j)}_\psi, \boldsymbol{\xi}^{(i)}), \tag{43}$$

then $\boldsymbol{p}$ is updated as

$$\boldsymbol{p}^{(i,j+1)} = \boldsymbol{p}^{(i,j)} - \delta^* \mathbf{E}_{i,j} \nabla_{\boldsymbol{p}} F^{(i,j)}_\psi. \tag{44}$$

When $\boldsymbol{p}$ converges, i.e., is updated to $\boldsymbol{p}^{(i+1,0)}$, the Lagrangian multipliers $\boldsymbol{\xi}$ are updated once based on the dual ascent method as

$$\boldsymbol{\xi}^{(a+1)} = \boldsymbol{\xi}^{(i)} + \nabla_{\boldsymbol{\xi}} F_\psi(\boldsymbol{p}^{(i+1,0)}, \boldsymbol{\xi}^{(i)}) \tag{45}$$

In brief, the algorithm for solving power allocation problem is presented in Algorithm 2. As seen that, the inner loop updates only $\boldsymbol{p}$, while the outer loop updates $\boldsymbol{p}$ to convergence and then updates $\boldsymbol{\xi}$ once until all variables converge to obtain the optimal $\boldsymbol{p}^*$.

Authorized licensed use limited to: JILIN UNIVERSITY. Downloaded on August 29,2025 at 04:28:18 UTC from IEEE Xplore. Restrictions apply.
© 2025 IEEE. All rights reserved, including rights for text and data mining and training of artificial intelligence and similar technologies. Personal use is permitted, but republication/redistribution requires IEEE permission. See https://www.ieee.org/publications/rights/index.html for more information.

This article has been accepted for publication in IEEE Internet of Things Journal. This is the author's version which has not been fully edited and content may change prior to final publication. Citation information: DOI 10.1109/JIOT.2025.3602496



**Algorithm 3** BCD Algorithm for Joint Optimization

**Input:** LED-user association $\boldsymbol{\lambda}^{(0)}$, power allocation $\boldsymbol{p}^{(0)}$, and iteration index $r$.
**Output:** Optimal LED-user association $\boldsymbol{\lambda}^*$, power allocation $\boldsymbol{p}^*$, and objective value $\psi^*$.
**Initialization:** Set iteration index $r = 0$, accuracy tolerance $\epsilon_4 = 10^{-4}$, and initialized $\boldsymbol{\lambda}^{(0)}, \boldsymbol{p}^{(0)}$;
**repeat**
  Fix $\boldsymbol{p}^{(r)}$, solve the problem $\mathbf{P_{1.1}}$ by Algorithm 1 to obtain the optimal solution denoted $\boldsymbol{\lambda}^{(r+1)}$;
  Fix $\boldsymbol{\lambda}^{(r+1)}$, solve the problem $\mathbf{P_{1.2}}$ by Algorithm 2 to obtain the optimal solution denoted $\boldsymbol{p}^{(r+1)}$;
  Calculate the objective function value $\psi^{(r+1)}$ by $\boldsymbol{\lambda}^{(r+1)}$, and $\boldsymbol{p}^{(r+1)}$;
  Set $r \leftarrow r + 1$;
**until** $|\psi^{(r)} - \psi^{(r-1)}| \leq \epsilon_4$;
**return** $\{\boldsymbol{\lambda}^*, \boldsymbol{p}^*, \psi^*\}$.

**Algorithm 4** DE-Based Optimization for RIS Placement

**Input:** Population size $N_p$, number of iterations $N_t$, and iteration index $i$.
**Output:** Optimal RIS array posiotn $\mathbf{w}^*$, RIS unit deployment $\boldsymbol{\zeta}^*$, LED-user association $\boldsymbol{\lambda}^*$, power allocation $\boldsymbol{p}^*$, and objective value $\psi^*$.
**Initialization:** Set initialized population $Pop$ of $N_p$ individuals;
**repeat**
  Generate trail individuals by mutation operation;
  Generate offspring by crossover operation;
  Optimize the joint optimization using Algorithm 3 for each individual to obtain fitness values $\{\psi\}$;
  Select better offspring to replace parent update $Pop$;
  Set $i \leftarrow i + 1$;
**until** $i > N_t$;
$\psi^* \leftarrow \max\{\psi\}$ and obtain $\{\mathbf{w}^*, \boldsymbol{\zeta}^*, \boldsymbol{\lambda}^*, \boldsymbol{p}^*\}$
**return** $\{\mathbf{w}^*, \boldsymbol{\zeta}^*, \boldsymbol{\lambda}^*, \boldsymbol{p}^*, \psi^*\}$.

### *D. BCD Method for Joint Optimization*

In this section, the joint LED-user association and power allocation problem is solved by BCD algorithm, with given RIS array position and RIS unit deployment. First, the LED-user association problem is solved by Algorithm 1 to obtain the association matrix $\boldsymbol{\lambda}$ with the optimized power vector $\boldsymbol{p}$. Then, the power allocation problem is solved by Algorithm 2 based on the optimized matrix $\boldsymbol{\lambda}$ to get vector $\boldsymbol{p}$. The algorithm terminates when objective value converges, i.e., $|\psi(i) - \psi^{(i-1)}|$ is less than a threshold. To sum up, the procedure of BCD algorithm is summarized in Algorithm 3.

To ensure the convergence of the BCD framework, each subproblem is solved to its near-optimal solution. Specifically, Algorithm 1 guarantees global optimality for the non-convex LED-user association subproblem, while Algorithm 2 aims for a high-quality local optimum for the non-convex power allocation subproblem by employing multiple initializations. The convergence of Algorithm 3 as follows:

$$\begin{aligned}\psi(\widehat{\mathbf{w}}, \widehat{\boldsymbol{\zeta}}, \boldsymbol{\lambda}^{(r)}, \boldsymbol{p}^{(r)}) &\overset{(a)}{\leq} \psi(\widehat{\mathbf{w}}, \widehat{\boldsymbol{\zeta}}, \boldsymbol{\lambda}^{(r+1)}, \boldsymbol{p}^{(r)}) \\ &\overset{(b)}{\leq} \psi(\widehat{\mathbf{w}}, \widehat{\boldsymbol{\zeta}}, \boldsymbol{\lambda}^{(r+1)}, \boldsymbol{p}^{(r+1)}),\end{aligned} \tag{46}$$

where $\psi(\widehat{\mathbf{w}}, \widehat{\boldsymbol{\zeta}}, \boldsymbol{\lambda}^{(r)}, \boldsymbol{p}^{(r)})$ is the objective function value at the $r$th iteration. In inequality (46)a, given the power allocation, the objective value is non-increasing after each iteration of Algorithm 1, as $\bar{v}_u$ converges and the optimal solution is reached. Similarly, inequality (46)b holds due to the sub-optimality of power allocation. Therefore, the objective function value of the joint optimization problem is always non-increasing, and is upper bounded by a finite value.

### *E. DE-Based optimization for RIS Placement*

The joint optimization problem is solved based on a fixed RIS array position and unit deployment. However, any changes to these parameters affect all objective functions and constraints. Since the position and deployment of the RIS units influence system performance, finding the optimal settings is crucial to maximizing the objective function value. The DE algorithm is well-suited for this, as it efficiently handles continuous solution spaces, regardless of the problem's nature. Specifically, the RIS placement problem, involving both continuous (position) and binary (unit deployment) variables, is a MINLP problem. DE's global search capability and inherent ability to manage mixed-integer variables make it a robust choice for exploring the complex and multimodal search space of this outer optimization layer, where traditional gradient-based methods or direct application of BCD to the full MINLP would struggle to find high-quality solutions.

The DE-based optimization starts with an initial population of $N_p$ individuals randomly generated within the search space, and explores it over $N_t$ iterations. The population first undergoes a mutation operation to generate $N_p$ trial individuals, followed by a crossover operation to produce offspring. However, since the unit deployment is binary variable, threshold rounding [33] is applied to convert the continuous variables into binary values before calculating the fitness. Specifically, for each element $\zeta_m$ representing whether $m$th mirror is deployed, if its continuous value generated by DE is greater than or equal to a predefined threshold (e.g., 0.5), it is rounded up to 1; otherwise, it is rounded down to 0. This ensures that $\zeta_m$ takes on its required binary value $\{0, 1\}$ before being used in the objective function calculation. Each individual corresponds to a specific RIS array position and unit deployment, and the optimal objective function value is computed using Algorithm 3, which serves as the fitness value for that individual. In each iteration, the offspring with the best fitness values replace the parents. The pseudocode for the DE algorithm is summarized in Algorithm 4.

The JPAPA (Algorithm 4) converges to a near-optimal solution with probability 1 as $N_t \to \infty$, satisfying:

$$\lim_{N_t \to \infty} P\left((\psi^* - \psi^{(N_t)}) \leq \varepsilon\right) = 1, \quad \forall \varepsilon > 0 \tag{47}$$

where $\psi^*$ is the global optimum.

*Proof.* The proof is given in Appendix C. □

Authorized licensed use limited to: JILIN UNIVERSITY. Downloaded on August 29,2025 at 04:28:18 UTC from IEEE Xplore. Restrictions apply.
© 2025 IEEE. All rights reserved, including rights for text and data mining and training of artificial intelligence and similar technologies. Personal use is permitted, but republication/redistribution requires IEEE permission. See https://www.ieee.org/publications/rights/index.html for more information.

This article has been accepted for publication in IEEE Internet of Things Journal. This is the author's version which has not been fully edited and content may change prior to final publication. Citation information: DOI 10.1109/JIOT.2025.3602496



### F. Computational Complexity Analysis

The computational complexity of solving problem $\mathbf{P_{1.1}}$ is $\mathfrak{O}_1 = \mathcal{O}(\max(L, 3U(U-1))^4\sqrt{L}\log(\frac{1}{\epsilon_1\xi}))$ based on SDR and PGD presented in Algorithm 1, where $\xi$ is the accuracy of PGD algorithm. Furthermore, problem $\mathbf{P_{1.2}}$ is solved based on the BFGS algorithm presented in Algorithm 2, and its computational complexity can be calculated as $\mathfrak{O}_2 = \mathcal{O}(\max(\log\frac{1}{\epsilon_2}, \log\frac{1}{\epsilon_3})LU)$. For the BCD algorithm in Algorithm 3, its computational complexity is $\mathfrak{O}_3 = \mathcal{O}((\mathfrak{O}_1 + \mathfrak{O}_2)\log\frac{1}{\epsilon_4})$.

Furthermore, in each iteration in Algorithm 4, the mutation, crossover, and selection steps of the DE algorithm have a complexity of $\mathcal{O}(N_p(3+M))$. The most computationally intensive part lies in the fitness evaluation, where each of the $N_p$ individuals is passed through Algorithm 3. Therefore, the total complexity of JPAPA over $N_t$ iterations is $\mathcal{O}(N_pN_t(3+M+\mathfrak{O}_3))$.

The computational complexity of the proposed JPAPA algorithm scales with the number of users ($U$), LEDs ($L$), and RIS units ($M$). The complexity increases significantly with $L$ due to the $L^4$ term in $\mathfrak{O}_1$, making the algorithm computationally expensive for large numbers of LEDs. The number of users also contributes to the complexity quadratically, as seen in the $U^2$ term. However, the algorithm's complexity with respect to $M$ is linear, which makes it more scalable for larger RIS configurations.

## V. Numerical Results

In this section, simulation results are presented to evaluate the effectiveness of the proposed approach for indoor VLC. Specifically, all the simulations are performed in MATLAB R2023a on a desktop computer equipped with an Intel(R) Core(TM) i5-12700KF CPU @ 2.20GHz 3.60GHz and 32 GB RAM.

### A. Simulation Setups

*1) Scenarios:* The dimensions of room are set to 5 m × 5 m × 3.5 m, and the area size of each RIS unit is 10 × 10 cm$^2$. The fixed positions of four LEDs are {(2, 2, 3.5), (3, 2, 3.5), (2, 3, 3.5), (3, 3, 3.5)}, while users are randomly distributed within the room positioned at a height of 1 m above the ground. The RIS array moves on the wall where the CC is located as shown in Fig. 1, i.e., the position of $m$th unit is $(x_m, 0, z_m)$. In addition, assuming that the user coordinates of *t* time slot are known, the optimal configuration under different time slots can be solved by using the solution method.

*2) Parameters:* The default values of the simulation parameters are listed in Table II. Most of the parameter values, such as LED semi-angle, PD area, optical filter gain, were chosen in accordance with widely adopted settings in prior works (e.g., [18], [23], [29]) to ensure fairness and comparability.

*3) Benchmarks:* This work evaluates the proposed JPAPA in comparison with the following methods and schemes.

- *DE* [37]: a basic DE algorithm solves the constrained optimization problem $\mathbf{P_1}$ without decomposition, chosen for its global optimization ability and relevance to our design. Its computational complexity is $\mathcal{O}(N_pN_t(3+M+LU+L)$.
- *Genetic algorithm (GA)* [38]: a basic GA algorithm solves the constrained optimization problem $\mathbf{P_1}$ without decomposition, widely used in RIS-related research for its simplicity and versatility. Its computational complexity is $\mathcal{O}(N_pN_t(1+(p_c+p_m)(3+M+LU+L))$, where $p_c$ and $p_m$ represent the cross probability and mutation probability, both of which are set to 0.5.
- *SHADE* [39]: an improved DE algorithm solves the constrained optimization problem $\mathbf{P_1}$ without decomposition, offering better convergence for complex problem. Its computational complexity is $\mathcal{O}(N_pN_t(3+M+LU+L)$.
- *PJAPA*: the unit deployment is fixed and the remaining configuration is the same as JPAPA.
- *DJAPA*: the array position is fixed and the remaining configuration is the same as JPAPA.
- *JPA-UPA*: each LED is allocated the same transmit power and the remaining configuration is the same as JPAPA.
- *JPA-FRPA* [40]: a fixed ratio, obtained by bisection search, is adopted to allocate the power.
- *JPA-NGDPA* [41]: the power allocation of LEDs is dynamically adjusted according to the multiusers channel gains.

Above three baseline evolutionary algorithms are chosen to demonstrate the advantages of our proposed decomposition-based joint optimization under fair computational budgets. The selection of the last five schemes is to demonstrate the effects of RIS placement, LED-user association and power allocation.

TABLE II
Simulation Parameters

| Parameter | Value |
|---|---|
| Number of LEDs, $L$ | 4 |
| Number of RIS units, $M$ | 36 |
| Half irradiation intensity semi-angle, $\Phi_{1/2}$ | 60° |
| Semi-angle of the FOV, $\Theta$ | 50° |
| Area of PD, $A_u$ | 1 cm$^2$ |
| Refractive index, $\eta$ | 1.5 |
| Reflection factor, $\rho$ | 0.95 |
| Optical filter gain, $g_c$ | 1.5 |
| Modulation bandwidth, $B$ | 20 MHz |
| Minimum QoS requirements, $R_{\min}$ | 1 Mbps |
| Noise power, $10\log\delta^2$ | -90 dB |
| Total power of LED, $p_{total}$ | 20 W |
| Population size of DE, $N_p$ | 50 |
| Number of iteration of DE, $N_t$ | 300 |

### B. Evaluation Results

*1) Convergence performance of the BCD and JPAPA:* The Fig. 4(a) illustrates the convergence performance of the BCD algorithm under varying configurations of the number of users ($U$) and RIS units ($M$). The convergence trend demonstrates that the BCD algorithm achieves stability within approximately 10 iterations, regardless of the specific $U$ and $M$. Larger RIS unit counts ($M = 49$) consistently yield higher objective values compared to smaller RIS configurations ($M = 36$ and $M = 25$), due to the enhanced beamforming capabilities. For the same $M$, scenarios with more users ($U = 4$)

Authorized licensed use limited to: JILIN UNIVERSITY. Downloaded on August 29,2025 at 04:28:18 UTC from IEEE Xplore. Restrictions apply.
© 2025 IEEE. All rights reserved, including rights for text and data mining and training of artificial intelligence and similar technologies. Personal use is permitted, but republication/redistribution requires IEEE permission. See https://www.ieee.org/publications/rights/index.html for more information.

This article has been accepted for publication in IEEE Internet of Things Journal. This is the author's version which has not been fully edited and content may change prior to final publication. Citation information: DOI 10.1109/JIOT.2025.3602496



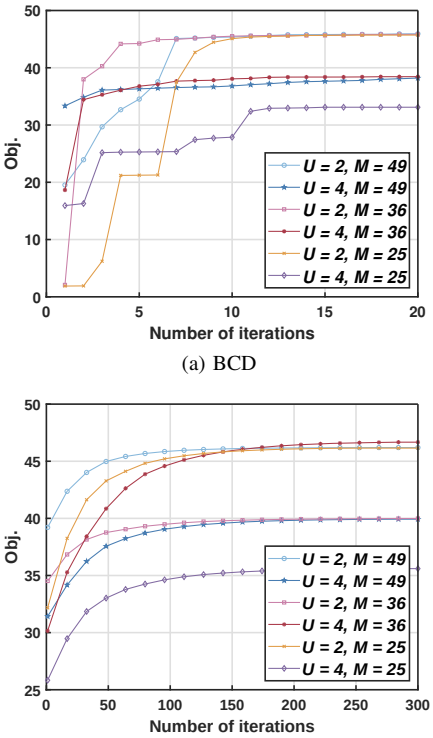


(a) BCD

(b) JPAPA

Fig. 4. Convergence of the BCD and JPAPA under different numbers of users and RIS units.

achieve slightly lower objective values compared to scenarios with fewer users ($U = 2$), highlighting the trade-off between sum-rate maximization and limited system resources. The convergence is notably slower and more irregular for smaller $M = 25$, particularly when $U = 4$, reflecting the algorithm's sensitivity to reduced degrees of freedom. Furthermore, all the curves exhibit a nondecreasing trend, which aligns with the theoretical analysis presented earlier in Section IV-D.

Furthermore, we additionally evaluate the convergence behavior of the entire JPAPA algorithm. As illustrated in Fig. 4(b), under different numbers of users $U$ and RIS units $M$, the objective value of JPAPA exhibits a clear non-decreasing trend and gradually approaches a steady state within a reasonable number of iterations. Compared with the BCD-only convergence shown in Fig. 4(a), the full JPAPA convergence curves reflect the additional optimization process introduced by the DE stage, which explores the RIS placement solution space. The results verify that the integration of the DE and BCD stages does not compromise convergence stability, and the algorithm consistently converges to high-quality solutions across all tested configurations.

*2) Performance comparison with three methods:* Table III presents the comparative results of optimization objectives obtained using different methods, including DE, GA, SHADE, and the proposed JPAPA. The table reports results for three scenarios with varying number of $U$ ($U = \{2, 3, 4\}$), and the comparison focuses on three metrics, i.e., objective function value (Obj.), SR ($SR$), and IU ($\Omega$). In addition, their running times $T$ are also provided separately.

TABLE III
COMPARISON RESULTS OF OPTIMIZATION OBJECTIVES OBTAINED BY DIFFERENT METHODS

| $U$ | Method | Obj. | $SR$ (Mbps) | $\Omega$ | $T$ (s) |
|---|---|---|---|---|---|
| 2 | DE | 46.13 | 64.62 | 0.1849 | **0.68** |
| | GA | 45.97 | **65.37** | 0.1940 | 0.88 |
| | SHADE | **46.21** | 64.59 | 0.1829 | 0.80 |
| | JPAPA | 46.11 | 64.46 | **0.1835** | 1.61 |
| 3 | DE | 42.68 | 64.22 | **0.2155** | **1.99** |
| | GA | -8.45 | 39.26 | 0.4771 | 2.57 |
| | SHADE | 24.89 | 49.39 | 0.2450 | 2.34 |
| | JPAPA | **45.81** | **69.63** | 0.2382 | 3.72 |
| 4 | DE | 29.11 | 51.83 | **0.2273** | **2.72** |
| | GA | -17.96 | 43.62 | 0.6158 | 3.52 |
| | SHADE | 23.58 | 53.49 | 0.2991 | 3.20 |
| | JPAPA | **38.52** | **67.99** | 0.2947 | 11.91 |

For $U = 2$, all methods achieve comparable Obj., with SHADE slightly outperforming others in Obj. (46.21), and GA achieving the highest $SR$ = 65.37 Mbps. However, JPAPA achieves the lowest $\Omega$ = 0.1835, indicating better lighting balance. Despite its more complex structure, the slightly longer runtime of JPAPA ($T$ = 1.61 s) remains acceptable given its balanced performance. As the number of users increases to $U = 3$, the advantages of JPAPA become more pronounced. JPAPA achieves the best performance across all metrics: highest Obj. (45.81), highest $SR$ (69.63 Mbps), and competitive $\Omega$ (0.2382). In contrast, GA performs poorly, even yielding a negative Obj. (-8.45), likely due to failing constraint satisfaction (e.g., rate or SIC order). SHADE and DE show degraded $SRs$ and higher $\Omega$ values, suggesting difficulty in navigating the expanded solution space as $U$ increases. When $U = 4$, the performance gap further widens. JPAPA maintains its advantage with Obj. = 38.52 and $SR$ = 67.99 Mbps, outperforming DE ($SR$ = 51.83) and SHADE ($SR$ = 53.49). Although the $\Omega$ of JPAPA increases to 0.2947, it remains within acceptable bounds and superior to GA and SHADE. Notably, the runtime $T$ of JPAPA highly increases to 10.91 s due to the higher problem dimensionality, increased variables for LED-user association and power allocation. However, this is justified by the substantial improvements in both $SR$ and Obj..

These results further verify the effectiveness and robustness of the proposed JPAPA algorithm, especially under high user-density scenarios where traditional evolutionary algorithms encounter difficulty due to the expanded and strongly coupled solution space. By leveraging decomposition-based joint optimization, JPAPA maintains high communication efficiency and illumination quality simultaneously. Although the computational complexity of JPAPA increases with the number of users, resulting in longer runtime, this is primarily due to the involvement of iterative convex optimization modules (e.g., SDR and BFGS) in solving high-dimensional subproblems. Nevertheless, the proposed method still achieves superior optimization performance and better trade-offs among SR and IU, which justifies the additional computational cost in practical deployments.

*3) Performance comparison with five schemes:* Table IV compares the performance of six different schemes under

Authorized licensed use limited to: JILIN UNIVERSITY. Downloaded on August 29,2025 at 04:28:18 UTC from IEEE Xplore. Restrictions apply.
© 2025 IEEE. All rights reserved, including rights for text and data mining and training of artificial intelligence and similar technologies. Personal use is permitted, but republication/redistribution requires IEEE permission. See https://www.ieee.org/publications/rights/index.html for more information.

This article has been accepted for publication in IEEE Internet of Things Journal. This is the author's version which has not been fully edited and content may change prior to final publication. Citation information: DOI 10.1109/JIOT.2025.3602496



TABLE IV
COMPARISON OF DIFFERENT SCHEMES FOR VARYING $U$.

| Method | $U = 2$ | | | $U = 3$ | | | $U = 4$ | | |
|---|---|---|---|---|---|---|---|---|---|
| | **Obj.** | $\boldsymbol{SR}$ (Mbps) | $\boldsymbol{\Omega}$ | **Obj.** | $\boldsymbol{SR}$ (Mbps) | $\boldsymbol{\Omega}$ | **Obj.** | $\boldsymbol{SR}$ (Mbps) | $\boldsymbol{\Omega}$ |
| PJAPA | 46.06 | 64.43 | 0.1837 | 40.53 | 58.95 | **0.1841** | 30.24 | 52.43 | **0.2219** |
| DJAPA | 45.58 | **64.70** | 0.1911 | 42.09 | 63.94 | 0.2185 | 34.83 | 59.75 | 0.2493 |
| JPA-UPA | - | - | - | - | - | - | - | - | - |
| JPA-FRPA | 16.00 | 55.14 | 0.3915 | 22.05 | 61.15 | 0.3910 | - | - | - |
| JPA-NGDPA | 36.12 | 59.58 | 0.2346 | 34.80 | 65.27 | 0.3048 | 33.51 | 61.59 | 0.2808 |
| JPAPA | **46.11** | 64.46 | **0.1835** | **45.81** | **69.63** | 0.2382 | **38.52** | **67.99** | 0.2947 |

varying numbers of users $U = \{2, 3, 4\}$, in terms of the Obj., SR, and $\Omega$. The schemes include PJAPA (fixed unit deployment), DJAPA (fixed array position), JPA-UPA (uniform power allocation), JPA-FRPA (fixed ratio power allocation), JPA-NGDPA (gain-based dynamic power allocation), and the proposed JPAPA. Note that "–" in the table indicates that the corresponding scheme failed to find a feasible solution under the constraints, and hence the results are not reported.

For $U = 2$, JPAPA outperforms all other schemes, achieving the highest Obj. of 46.11 and the lowest $\Omega = 0.1835$, indicating excellent joint performance in communication and illumination. DJAPA also achieves a relatively high $SR$ (64.70 Mbps), but with inferior $\Omega = 0.2143$, reflecting uneven illumination due to its fixed RIS position. JPA-FRPA and JPA-NGDPA achieve feasible results but suffer from poorer trade-offs, either due to rigid power allocation ratios or power concentration effects. Notably, JPA-UPA fails to find a feasible solution even for $U = 2$, suggesting that uniform power allocation lacks sufficient flexibility to satisfy multiple joint constraints simultaneously, even under moderate user load. When $U = 3$, JPAPA maintains clear superiority, achieving Obj. = 45.81, $SR$ = 69.63 Mbps, and $\Omega = 0.2382$. This demonstrates the benefits of jointly optimizing RIS position and deployment structure. In contrast, JPA-UPA again fails to produce a feasible result, while JPA-NGDPA, although achieving a high $SR$ (65.27 Mbps), shows a significantly degraded $\Omega = 0.3048$ due to its aggressive power steering. DJAPA and PJAPA perform reasonably but remain suboptimal in both objectives. As $U$ increases to 4, system resource contention intensifies. JPAPA still delivers the best overall results, Obj. = 38.52, $SR$ = 67.99 Mbps, $\Omega = 0.2947$, showcasing its robustness under user load. JPA-FRPA, while previously feasible, fails to converge to a feasible solution under $U = 4$ due to stricter illumination and QoS constraints. Similarly, JPA-UPA continues to be infeasible. This underscores that simple or inflexible power control strategies are ill-suited for dense user environments. Only JPAPA effectively manages resource coupling across communication and lighting demands under these conditions.

In summary, the results demonstrate that JPAPA, by jointly optimizing RIS position, unit deployment, user association, and power allocation, consistently achieves the best trade-off between communication throughput and illumination quality. The increasing infeasibility of baseline schemes under higher $U$ further highlights the importance of coordinated and adaptive optimization in dense VLC systems.

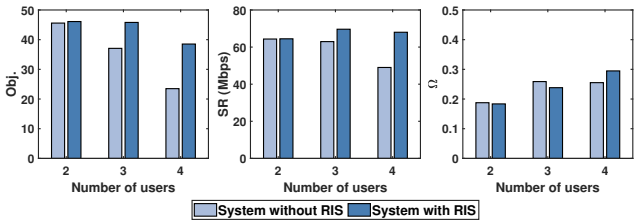


Fig. 5. System (with/without RIS) performance with different numbers of users.

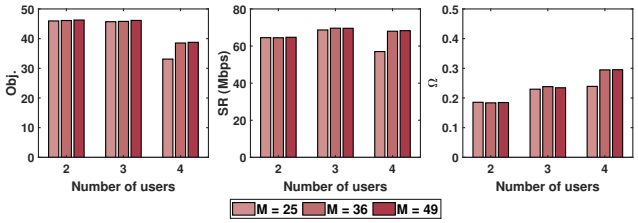


Fig. 6. System performance with different amount of RIS units.

*4) Impact of Number of RIS units:* Fig. 5 compares system performance with and without RIS under a fixed number of RIS units ($M = 36$), across varying user scenarios ($U = \{2, 3, 4\}$). It is evident that the deployment of RIS substantially improves overall system performance. Specifically, both the Obj. and $SR$ are significantly higher in the system with RIS, especially when $U = 3$ and $U = 4$, demonstrating the RIS's ability to alleviate signal blockage and enhance multi-user channel conditions. Moreover, the system with RIS achieves better IU (i.e., lower $\Omega$) in most cases, particularly for fewer users. However, as $U$ increases to 4, a slight rise in $\Omega$ is observed, indicating a trade-off between communication and illumination due to increased user competition and spatial interference.

Fig. 6 further analyzes the impact of the RIS unit count ($M = \{25, 36, 49\}$). Increasing $M$ leads to consistent improvements in Obj. and $SR$ for all user scenarios, with the gains becoming more pronounced as the number of users increases. For example, under $U = 4$, moving from $M = 25$ to $M = 49$ leads to a significant $SR$ improvement, showing that a larger number of units can better manage user interference and spatial diversity. However, as $M$ increases, $\Omega$ also shows an upward trend, indicating that although communication performance benefits from more RIS units, the illumination uniformity slightly degrades. This is likely due to

Authorized licensed use limited to: JILIN UNIVERSITY. Downloaded on August 29,2025 at 04:28:18 UTC from IEEE Xplore. Restrictions apply.
© 2025 IEEE. All rights reserved, including rights for text and data mining and training of artificial intelligence and similar technologies. Personal use is permitted, but republication/redistribution requires IEEE permission. See https://www.ieee.org/publications/rights/index.html for more information.

This article has been accepted for publication in IEEE Internet of Things Journal. This is the author's version which has not been fully edited and content may change prior to final publication. Citation information: DOI 10.1109/JIOT.2025.3602496



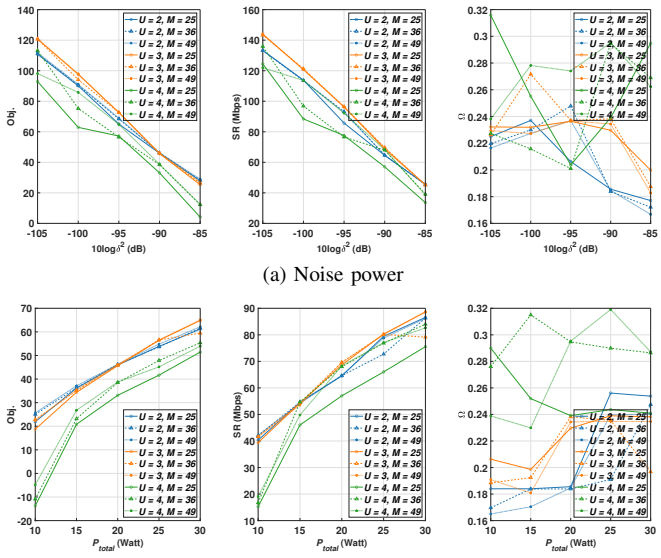


(a) Noise power

(b) LED total power

Fig. 7. Impact of noise power and LED total power on system performance.

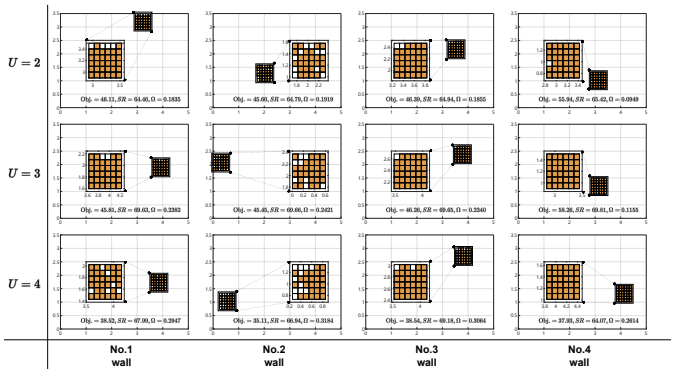


Fig. 8. RIS array position and deployment in four walls for different numbers of users.

the intensified focusing effect from highly reflective surfaces, which results in less evenly distributed light. Nonetheless, as $M$ increases from 36 to 49, the performance gains begin to saturate, suggesting a diminishing return. This performance bottleneck may arise from the physical deployment limits and overlapping reflective paths, which reduce the marginal benefit of additional RIS units.

*5) Impact of noise and total power:* Fig. 7(a) illustrates the impact of noise power on system performance under different user numbers ($U = \{2, 3, 4\}$) and RIS unit numbers ($M = \{25, 36, 49\}$). As noise power increases (-105 dB to -85 dB), both the Obj. and $SR$ decrease markedly. Systems with fewer users ($U = 2$) consistently achieve higher Obj. and $SR$, since multi-user interference is lower and resource allocation is simpler. Additionally, configurations with more RIS units ($M = 49$ and $M = 25$) exhibit superior performance compared to $M = 25$, as increased RIS units enhance NLoS channel gains, improving both SINR and illumination distribution.

Fig. 7(b) shows the effect of increasing LED total power ($p_{total}$) on performance. Both Obj. and $SR$ steadily improve as $p_{total}$ increases from 10 Watt to 30 Watt, though the improvement rate slows at higher power levels, indicating saturation. Larger $M$ values again provide performance gains due to better control over reflected light. Systems with $U = 2$ achieve the best results, while $U = 4$ initially lags but narrows the gap at high power levels.

The $\Omega$ exhibits non-monotonic fluctuations under both varying noise power and total LED power, especially in scenarios with larger $U$ and $M$. This behavior can be attributed to several interrelated factors. First, the inherent trade-off in multi-objective optimization means that JPAPA may prioritize improving SR at the expense of IU, particularly under high noise or limited power, leading to uneven illumination and increased variance. Second, RIS unit deployment ($\zeta$) involves discrete decisions (0/1), so even small changes in system conditions can cause abrupt shifts in the reflection paths, further amplifying fluctuations in $\Omega$. Third, as the $M$ increases, so does the flexibility in adjusting reflected light, but this also introduces complex interference patterns that may lead to localized over-illumination. In multi-user scenarios, the system may favor high-priority users when allocating resources, causing spatial imbalance in illumination. Finally, the IU constraint ensures a minimum illuminance at each monitoring point, but higher $p_{total}$ can result in some regions being excessively illuminated without proportionate improvement elsewhere, thereby increasing the overall luminance variance and the value of $\Omega$.

Overall, Fig. 7 highlights that noise power, LED total power, and RIS unit number jointly influence SR and IU. Although higher $M$ and $p_{total}$ improve overall performance, they also increase optimization complexity and the risk of non-uniform illumination, especially in multi-user scenarios.

*6) Performance of RIS placed on different wall:* Fig. 8 visualizes the ideal position and unit deployment of the RIS array on different walls under different user numbers ($U = \{2,3,4\}$), and the colored grid cells represent RIS unit with mirror. No.1 wall is the default wall for RIS placement, No.2 wall is adjacent to No.1 wall on the left, No.3 wall is opposite to No.1 wall, and No.4 is is adjacent to No.1 wall on the right. As shown, when the RIS is placed on No.4 wall, the best performance in terms of both SR and IU is achieved with 2 and 3 users, although this configuration requires the deployment of the most mirrors. This means that better system performance is achieved at the same time that deployment costs are increased. However, when the number of users is equal to 4, it gets the worst SR but the best IU. Therefore, during the deployment process, it is crucial to consider multiple factors, including system performance, deployment cost, and user requirements, to achieve an ideal balance.

Fig. 9 shows the effect of the error in CSI on the system performance. We vary the variance of the CSI error $\sigma_e^2$ between -200 dB and -20 dB [21]. Note that $\sigma_e^2 = 0$ corresponds to the perfect CSI scenario. We plot the achievable $SR$ versus the error variance $\sigma_e^2$ with $U$ = 4, $M$ = 36, $p_{total} = 20$ Watt, and noise $10 \log \delta^2 = -90$ dB for the proposed JPAPA. Under perfect CSI, the SR remains stable at approximately 67.99 Mbps. However, the system performance is highly affected by the increase of the CSI error. For example, with $\sigma_e^2 = -140$

Authorized licensed use limited to: JILIN UNIVERSITY. Downloaded on August 29,2025 at 04:28:18 UTC from IEEE Xplore. Restrictions apply.
© 2025 IEEE. All rights reserved, including rights for text and data mining and training of artificial intelligence and similar technologies. Personal use is permitted, but republication/redistribution requires IEEE permission. See https://www.ieee.org/publications/rights/index.html for more information.

This article has been accepted for publication in IEEE Internet of Things Journal. This is the author's version which has not been fully edited and content may change prior to final publication. Citation information: DOI 10.1109/JIOT.2025.3602496



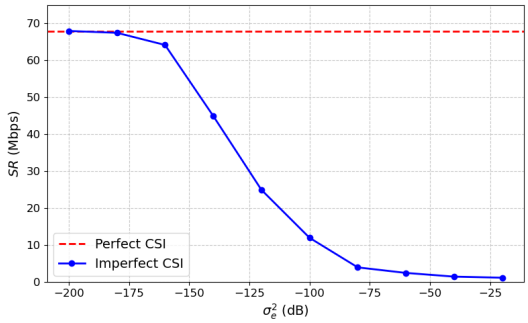


Fig. 9. Achieved $SR$ as a function of $\sigma_e^2$ under imperfect CSI.

dB the SR drops to around 45 Mbps, and at $\sigma_e^2 = -100$ dB, it decreases further to about 12 Mbps, representing a 5-6× reduction compared to the perfect CSI case. Nevertheless, even under large errors, e.g., -60 dB, the algorithm maintains a non-zero $SR$ (about 1-2 Mbps), showing the robustness of the proposed JPAPA under challenging conditions.

## VI. Conclusion

This paper presents a novel approach to enhance the performance of RIS-assisted NOMA-based VLC systems by simultaneously optimizing both SR and IU. Unlike existing studies, this work incorporates RIS placement, encompassing both the position and unit deployment, as a key optimization variable. Additionally, LED-user association and power allocation are jointly optimized to address critical challenges such as signal blockage, interference, and uneven illumination in VLC systems. The optimization problem is formulated as a non-convex MINLP problem and solved using the proposed JPAPA approach. Simulation results demonstrate the superior performance of the proposed JPAPA compared to baseline methods. Optimized RIS placement significantly improves both SR and IU, with the system outperforming configurations without RIS placement optimization. The addition of RIS units notably enhances system performance, especially in multi-user scenarios. However, diminishing returns are observed, suggesting practical limits on deployment density. Furthermore, noise power and LED transmit power were found to have a substantial impact on both SR and IU, providing valuable insights for selecting ideal communication parameters in practical VLC deployments. This work establishes a foundational framework for integrating RIS and NOMA technologies into VLC systems, highlighting the importance of a carefully designed RIS placement strategy. Furthermore, it is important to acknowledge that while our proposed algorithm demonstrates significant performance gains, its computational complexity, particularly the notable scaling with the number of LEDs ($L$), poses a practical limitation for very large-scale VLC deployments. Future work will therefore focus on developing more computationally efficient algorithms or approximation techniques to enhance the scalability of our approach for systems with a high density of LEDs. And, future research could build upon this framework by exploring dynamic and adaptive RIS configurations, integrating additional performance metrics such as EE and latency, and conducting real-world experimental validations across a variety of indoor environments.

## Appendix A
## Proof of Theorem 1

To simplify the analysis, by fixing the RIS array position, unit deployment, and LED power allocation, the original problem $\mathbf{P}$ is simplified as follows:

$$\mathbf{P}': \quad \max_{\boldsymbol{\lambda}} SR \tag{48a}$$

$$\text{s.t.} \quad (13b), (13d), (13f), (13g). \tag{48b}$$

Since all other variables are fixed, $\Omega$ is determined, and the problem focuses solely on maximizing $SR$.

This optimization problem $\mathbf{P}'$ is essentially a 0-1 quadratic programming problem [42], which is NP-hard, as the constraint in (13f) involves $\boldsymbol{\lambda}$ taking binary values. Consequently, the original problem $\mathbf{P}$ with its additional complexity, is also NP-hard. Furthermore, $\mathbf{P}$ involves both binary variables (i.e., unit deployment $\boldsymbol{\zeta}$ and LED-user association $\boldsymbol{\lambda}$) and continuous variables (i.e., RIS array position $\mathbf{w}$ and LED power allocation $\boldsymbol{p}$), with non-convex constraints (e,g., in (13b), (13d), and (13h)). Therefore, $\mathbf{P}$ is an NP-hard non-convex MINLP problem.

## Appendix B
## Proof of Theorem 2

Since $\mathbf{D} = \tilde{\boldsymbol{\lambda}}\tilde{\boldsymbol{\lambda}}^\top$, the constraint (25e) can be given as

$$\mathbf{A}\tilde{\boldsymbol{\lambda}}\tilde{\boldsymbol{\lambda}}^\top \mathbf{1}_{LU\times 1} \le \mathbf{1}_{L\times 1}, \tag{49}$$

where $\tilde{\boldsymbol{\lambda}}^\top \mathbf{1}_{LU\times 1} = \sum_{i=1}^{LU} \tilde{\lambda}_i$ ,denoted a constant $c$. Specifically, the $i$th component of $\mathbf{A}\tilde{\boldsymbol{\lambda}}$ is

$$(\mathbf{A}\tilde{\boldsymbol{\lambda}})_i = \sum_{j=(i-1)L+1}^{iL} \tilde{\lambda}_j. \tag{50}$$

We consider two conditions that make the constraint (49) hold:

- If $c \ge 1$, obviously, $\mathbf{A}\tilde{\boldsymbol{\lambda}} \le \mathbf{1}_{L\times 1}$ must be satisfied.
- If $c < 1$, due to $(\mathbf{A}\tilde{\boldsymbol{\lambda}})_i \le c, \forall 1 \le i \le LU$, $\mathbf{A}\tilde{\boldsymbol{\lambda}} < \mathbf{1}_{L\times 1}$ must hold.

According to the above analysis, it can be concluded that if constraint (25e) holds, constraint (24e) also holds.

## Appendix C

The DE-based optimization in JPAPA consists of:

1) Population evolution: The mutation/crossover operations generate trial vectors $\mathbf{v}_i = \mathbf{w}_i + F \cdot (\mathbf{w}_{r1} - \mathbf{w}_{r2})$, where $\mathbf{w}_i$ is the parental individual and $F$ is the scaling factor.
2) Selection: The greedy selection $\mathbf{w}_i^{(t+1)} = \arg\max(\psi(\mathbf{w}_i^{(t)}), \psi(\mathbf{v}_i))$ ensures monotonic improvement, which satisfies:
$$\psi^{(t+1)} \ge \psi^{(t)}, \quad \forall t \ge 0 \tag{51}$$
3) BCD algorithm (Algorithm 3): As proven in Section IV-D, each BCD call converges to a local optimum $\psi^*_{\text{local}}$ for given $(\mathbf{w}, \boldsymbol{\zeta})$.

Authorized licensed use limited to: JILIN UNIVERSITY. Downloaded on August 29,2025 at 04:28:18 UTC from IEEE Xplore. Restrictions apply.
© 2025 IEEE. All rights reserved, including rights for text and data mining and training of artificial intelligence and similar technologies. Personal use is permitted, but republication/redistribution requires IEEE permission. See https://www.ieee.org/publications/rights/index.html for more information.

This article has been accepted for publication in IEEE Internet of Things Journal. This is the author's version which has not been fully edited and content may change prior to final publication. Citation information: DOI 10.1109/JIOT.2025.3602496



By the global convergence property of DE, when $N_t \to \infty$, the population almost surely contains solutions arbitrarily close to $\psi^*$. Combining with BCD convergence, it satisfies:

$$P\left((\psi^* - \psi^{(N_t)}) \leq \varepsilon\right) \geq 1 - e^{-\kappa N_t}, \quad \kappa > 0 \tag{52}$$

## REFERENCES


[1] D. Karunatilaka, F. Zafar, V. Kalavally, and R. Parthiban, "LED based indoor visible light communications: State of the art," *IEEE Commun. Surveys Tuts.*, vol. 17, no. 3, pp. 1649–1678, 2015.

[2] R. Zhu, M. Van den Abeele, J. Beysens, J. Yang, and Q. Wang, "Centimeter-level indoor visible light positioning," *IEEE Commun. Mag.*, vol. 62, no. 3, pp. 48–53, 2024.

[3] X. Wei, H. Guo, X. Wang, X. Wang, and M. Qiu, "Reliable data collection techniques in underwater wireless sensor networks: A survey," *IEEE Commun. Surveys Tuts.*, vol. 24, no. 1, pp. 404–431, 2022.

[4] P. Sharda, G. S. Reddy, M. R. Bhatnagar, and Z. Ghassemlooy, "A comprehensive modeling of vehicle-to-vehicle based VLC system under practical considerations, an investigation of performance, and diversity property," *IEEE Trans. Commun.*, vol. 70, no. 5, pp. 3320–3332, 2022.

[5] L. Yin, W. O. Popoola, X. Wu, and H. Haas, "Performance evaluation of non-orthogonal multiple access in visible light communication," *IEEE Trans. Commun.*, vol. 64, no. 12, pp. 5162–5175, 2016.

[6] H. Yang, W.-D. Zhong, C. Chen, A. Alphones, and P. Du, "QoS-driven optimized design-based integrated visible light communication and positioning for indoor IoT networks," *IEEE Internet Things J.*, vol. 7, no. 1, pp. 269–283, 2020.

[7] M. Obeed, A. M. Salhab, M.-S. Alouini, and S. A. Zummo, "On optimizing VLC networks for downlink multi-user transmission: A survey," *IEEE Commun. Surveys Tuts.*, vol. 21, no. 3, pp. 2947–2976, 2019.

[8] S. Aboagye, A. R. Ndjiongue, T. M. N. Ngatched, O. A. Dobre, and H. V. Poor, "RIS-assisted visible light communication systems: A tutorial," *IEEE Commun. Surveys Tuts.*, vol. 25, no. 1, pp. 251–288, 2023.

[9] B. Zhang, K. Yang, K. Wang, and G. Zhang, "Performance analysis for RIS-assisted SWIPT-enabled IoT systems," *IEEE Trans. Wireless Commun.*, vol. 23, no. 8, pp. 10 030–10 043, 2024.

[10] T. Wang, F. Yang, J. Song, and Z. Han, "Dimming techniques of visible light communications for human-centric illumination networks: State-of-the-art, challenges, and trends," *IEEE Wireless Commun.*, vol. 27, no. 4, pp. 88–95, 2020.

[11] C. Zhang, Y. Liu, J. Hu, and K. Yang, "Joint user identification, channel estimation, and data detection for grant-free NOMA in LEO satellite communications," *IEEE J. Sel. Areas Commun.*, vol. 43, no. 1, pp. 107–121, 2025.

[12] H. Abumarshoud, C. Chen, I. Tavakkolnia, H. Haas, and M. A. Imran, "Intelligent reflecting surfaces for enhanced physical layer security in NOMA VLC systems," in *Proc. IEEE Int. Conf. Commun. (ICC)*, 2023, pp. 3284–3289.

[13] Z. Liu, F. Yang, S. Sun, J. Song, and Z. Han, "Physical layer security in NOMA-based VLC systems with optical intelligent reflecting surface: A max-min secrecy data rate perspective," *IEEE Internet Things J.*, vol. 12, no. 6, pp. 7180–7194, 2025.

[14] H. Abumarshoud, B. Selim, M. Tatipamula, and H. Haas, "Intelligent reflecting surfaces for enhanced NOMA-based visible light communications," in *Proc. IEEE Int. Conf. Commun. (ICC)*, 2022, pp. 571–576.

[15] O. Maraqa, S. Aboagye, and T. M. N. Ngatched, "Optical STAR-RIS-aided VLC systems: RSMA versus NOMA," *IEEE Open J. Commun. Soc.*, vol. 5, pp. 430–441, 2024.

[16] A. Salehiyan and M. J. Emadi, "Performance analysis of uplink optical wireless communications in the presence of a simultaneously transmitting and reflecting reconfigurable intelligent surface," *IET Optoelectron.*, vol. 17, no. 4, pp. 129–138, 2023.

[17] Z. Liu, F. Yang, S. Sun, J. Song, and Z. Han, "Sum rate maximization for NOMA-based VLC with optical intelligent reflecting surface," *IEEE Wireless Commun. Lett.*, vol. 12, no. 5, pp. 848–852, 2023.

[18] Z. Liu, F. Yang, J. Song, and Z. Han, "NOMA-based MISO visible light communication systems with optical intelligent reflecting surface: Joint active and passive beamforming design," *IEEE Internet Things J.*, vol. 11, no. 10, pp. 18 753–18 767, 2024.

[19] C. Liu, L. Yu, X. Yu, J. Qian, Y. Wang, and Z. Wang, "Capacity analysis of RIS-assisted visible light communication systems with hybrid NOMA," in *Proc. IEEE Global Commun. Conf. (GLOBECOM) Workshops*, 2022, pp. 118–123.

[20] O. Maraqa and T. M. N. Ngatched, "Optimized design of joint mirror array and liquid crystal-based RIS-aided VLC systems," *IEEE Photonics J.*, vol. 15, no. 4, pp. 1–11, 2023.

[21] S. Ibne Mushfique, A. Alsharoa, and M. Yuksel, "MirrorVLC: Optimal mirror placement for multielement VLC networks," *IEEE Trans. Wireless Commun.*, vol. 21, no. 11, pp. 10 050–10 064, 2022.

[22] S. Sun, F. Yang, J. Song, and Z. Han, "Joint resource management for intelligent reflecting surface–aided visible light communications," *IEEE Trans. Wireless Commun.*, vol. 21, no. 8, pp. 6508–6522, 2022.

[23] N. An, F. Yang, L. Cheng, J. Song, and Z. Han, "IRS-assisted aggregated VLC-RF system: Resource allocation for energy efficiency maximization," *IEEE Trans. Wireless Commun.*, vol. 23, no. 10, pp. 12 578–12 593, 2024.

[24] M. D. Soltani, A. A. Purwita, Z. Zeng, H. Haas, and M. Safari, "Modeling the random orientation of mobile devices: Measurement, analysis and LiFi use case," *IEEE Trans. Commun.*, vol. 67, no. 3, pp. 2157–2172, 2019.

[25] A. M. Abdelhady, A. K. S. Salem, O. Amin, B. Shihada, and M.-S. Alouini, "Visible light communications via intelligent reflecting surfaces: Metasurfaces vs mirror arrays," *IEEE Open J. Commun. Soc.*, vol. 2, pp. 1–20, 2021.

[26] K.-H. Park, H. M. Oubei, W. G. Alheadary, B. S. Ooi, and M.-S. Alouini, "A novel mirror-aided non-imaging receiver for indoor $2 \times 2$ MIMO-visible light communication systems," *IEEE Trans. Wireless Commun.*, vol. 16, no. 9, pp. 5630–5643, 2017.

[27] S. Aboagye, T. M. N. Ngatched, O. A. Dobre, and A. R. Ndjiongue, "Intelligent reflecting surface-aided indoor visible light communication systems," *IEEE Commun. Lett.*, vol. 25, no. 12, pp. 3913–3917, 2021.

[28] A. Chaaban, Z. Rezki, and M.-S. Alouini, "On the capacity of the intensity-modulation direct-detection optical broadcast channel," *IEEE Trans. Wireless Commun.*, vol. 15, no. 5, pp. 3114–3130, 2016.

[29] S. Ibne Mushfique, A. Alsharoa, and M. Yuksel, "Mirrorvlc: Optimal mirror placement for multielement vlc networks," *IEEE Transactions on Wireless Communications*, vol. 21, no. 11, pp. 10 050–10 064, 2022.

[30] F. Wang, F. Yang, C. Pan, J. Song, and Z. Han, "Joint illumination and communication optimization in indoor VLC for IoT applications," *IEEE Internet Things J.*, vol. 9, no. 21, pp. 20 788–20 800, 2022.

[31] I. Alsyouf and S. Hamdan, "A multi-objective optimization of maintenance policies using weighted comprehensive criterion method (wccm)," in *Proc. 7th Int. Conf. Model. Simul. Appl. Optim. (ICMSAO)*, 2017, pp. 1–4.

[32] G. Sun, Y. Wang, Z. Sun, Q. Wu, J. Kang, D. Niyato, and V. C. M. Leung, "Multi-objective optimization for multi-UAV-assisted mobile edge computing," *IEEE Trans. Mob. Comput.*, vol. 23, no. 12, pp. 14 803–14 820, 2024.

[33] K. Elbassioni and S. Ray, "Threshold rounding for the standard LP relaxation of some geometric stabbing problems," *arXiv preprint arXiv:2106.12385*, 2021.

[34] S. Bubeck *et al.*, "Convex optimization: Algorithms and complexity," *Found. Trends Mach. Learn.*, vol. 8, no. 3-4, pp. 231–357, 2015.

[35] R. Zhao, W. B. Haskell, and V. Y. F. Tan, "Stochastic L-BFGS: Improved convergence rates and practical acceleration strategies," *IEEE Trans. Signal Process.*, vol. 66, no. 5, pp. 1155–1169, 2018.

[36] S. M. Asad and A. Zerguine, "Convergence analysis of a modified Armijo rule step-size LMF algorithm," in *Proc. Int. Conf. Inf. Sci. Signal Process. Their Appl. (ISSPA)*, 2012, pp. 343–347.

[37] Y. Chen, W. Li, J. Huang, H. Gao, and S. Deng, "A differential evolution offloading strategy for latency and privacy sensitive tasks with federated local-edge-cloud collaboration," *ACM Trans. Sens. Netw.*, 2024.

[38] S. Abdeljabar, M. W. Eltokhey, and M.-S. Alouini, "Sum rate and fairness optimization in RIS-assisted VLC systems," *IEEE Open J. Commun. Soc.*, vol. 5, pp. 2555–2566, 2024.

[39] W. Li, B. Sun, Y. Sun, Y. Huang, Y.-m. Cheung, and F. Gu, "DC-SHADE-IF: An infeasible–feasible regions constrained optimization approach with diversity controller," *Expert Syst. Appl.*, vol. 224, p. 119999, 2023.

[40] H. Marshoud, P. C. Sofotasios, S. Muhaidat, G. K. Karagiannidis, and B. S. Sharif, "On the performance of visible light communication systems with non-orthogonal multiple access," *IEEE Trans. Wireless Commun.*, vol. 16, no. 10, pp. 6350–6364, 2017.

[41] C. Chen, W.-D. Zhong, H. Yang, and P. Du, "On the performance of MIMO-NOMA-based visible light communication systems," *IEEE Photon. Technol. Lett.*, vol. 30, no. 4, pp. 307–310, 2018.

[42] A. Liefooghe, S. Verel, and J.-K. Hao, "A hybrid metaheuristic for multiobjective unconstrained binary quadratic programming," *Appl. Soft Comput.*, vol. 16, pp. 10–19, 2014.


Authorized licensed use limited to: JILIN UNIVERSITY. Downloaded on August 29,2025 at 04:28:18 UTC from IEEE Xplore. Restrictions apply.
© 2025 IEEE. All rights reserved, including rights for text and data mining and training of artificial intelligence and similar technologies. Personal use is permitted, but republication/redistribution requires IEEE permission. See https://www.ieee.org/publications/rights/index.html for more information.

This article has been accepted for publication in IEEE Internet of Things Journal. This is the author's version which has not been fully edited and content may change prior to final publication. Citation information: DOI 10.1109/JIOT.2025.3602496



**Xingwang Wang** received his Ph.D. in Engineering from Jilin University in 2018. After that, he joined Jilin University as an associate professor in 2020. His research interests cover cloud computing, the Internet of Things, underwater sensor networks, and deep learning.

**Junhong Huang** is currently working toward the Ph.D. degree in College of Computer Science and Technology, Jilin University. His research interest include wireless networks and communications, visible light communication, and the Internet of Things.

**Yafeng Sun** is currently working toward the Ph.D. degree in College of Computer Science and Technology, Jilin University. His research interest covers mobile computing, deep learning and evolutionary computing.

**Jiatong Tu** is currently working toward the M.E. degree in College of Computer Science and Technology, Jilin University. Her research interests include acoustic separation and underwater sensor networks.

**Kun Yang** (Fellow, IEEE) received the Ph.D. degree from the Department of Electronic and Electrical Engineering, University College London, London, U.K. He is currently a Chair Professor with the School of Computer Science and Electronic Engineering, University of Essex, Colchester, U.K.. He is also an affiliated Professor of Nanjing University, Nanjing, China. His main research interests include wireless networks and communications, future Internet, and edge computing. In particular he is interested in energy aspects of future communication systems, such as 6G and new artificial intelligence technique for wireless. He is a Member of Academia Europaea, a Fellow of IET, and a Distinguished Member of ACM.

Authorized licensed use limited to: JILIN UNIVERSITY. Downloaded on August 29,2025 at 04:28:18 UTC from IEEE Xplore. Restrictions apply.
© 2025 IEEE. All rights reserved, including rights for text and data mining and training of artificial intelligence and similar technologies. Personal use is permitted, but republication/redistribution requires IEEE permission. See https://www.ieee.org/publications/rights/index.html for more information.